Soil Dynamics and Earthquake Engineering 198 (2025) 109608

Contents lists available at ScienceDirect

Soil Dynamics and Earthquake Engineering

journal homepage: www.elsevier.com/locate/soildyn

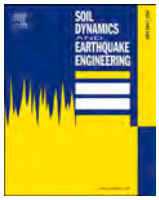

Examination of the severe impact of the February 6, 2023 earthquakes on Antakya district considering pulse-like ground motions, supershear rupture, and basin effects

Emre Gani [a,*], Sezer Öztürk [b], Ali Sarı [a]

[a] Department of Civil Engineering, Istanbul Technical University, ITU Ayazaga Campus, Maslak, Istanbul, 34469, Türkiye
[b] Department of Civil Engineering, Fatih Sultan Mehmet Vakif University, Merkezefendi, Mevlevihane Rd., No.27 Zeytinburnu, Istanbul, 34015, Türkiye

ARTICLE INFO

Keywords:
Supershear rupture
Forward directivity
Basin effect
Vertical earthquake
Structural damage

ABSTRACT

The first earthquake of the February 6 Kahramanmaraş sequence, with its epicenter in Pazarcık, caused severe damage and destruction in the Antakya/Hatay region. In addition to human factors such as structural design, construction practices, and inspection processes, the catastrophic outcomes were influenced by extraordinary seismic characteristics tied to the region's tectonics, geographic location, geological structure, and topographic features. The Antakya region has the potential to experience phenomena such as forward directivity, fling-step, supershear rupture, basin effects, and trampoline effects. This study analyzed records from strong ground motion stations in Antakya to investigate the signatures of these phenomena, both individually and in combination, providing a broader perspective compared to existing studies in the literature. Data from each station were evaluated based on the detection and orientation of velocity pulses, the shape of acceleration response spectra, Cumulative Absolute Velocity (CAV) values, Husid plots, and geological/topographic characteristics. The results revealed that some stations exhibited combined traces of forward directivity, supershear, and basin effects, while others displayed these effects individually. Additionally, heavy damage and destruction rates in neighborhoods surrounding each station were compiled. During the damage assessment, structures were categorized based on parameters such as building age, number of stories, and soil type. The findings showed a significant increase in heavy damage and destruction in cases where potential supershear, forward directivity, and basin effects occurred simultaneously. The use of the $V_{s,30}$-based soil classification and acceleration amplification approach was found to be inadequate in scenarios where basin and trampoline effects were likely. Furthermore, the discrepancy between the response spectra of the Turkish Building Earthquake Code 2018 (TBEC-2018) and station records can be attributed to pulse-like ground motions, supershear effects, and site amplifications. Therefore, it is crucial to consider these phenomena in the design and assessment processes for both newly constructed and existing buildings in regions where such effects are likely to occur.

1. Introduction

Türkiye is located in one of the most seismically active regions in the world, where numerous destructive earthquakes have occurred throughout history. Notable examples include the 1992 Erzincan, 1999 Kocaeli, 2011 Van, and 2020 Elazığ earthquakes. Most recently, the twin earthquakes of February 6, 2023, in Kahramanmaraş caused the deaths of over 53,000 people and left more than 107,000 injured. These earthquakes, regarded as one of the most significant disasters in recent years, have led to studies that analyzed strong ground motion records to investigate the earthquake's characteristic features [1–5]. In addition, many studies have examined the structural damage and collapse caused by earthquakes using data collected from field surveys and inspections. The literature includes investigations of the damage to conventional multi-story, multi-span reinforced concrete buildings [6–9], as well as studies focusing on various other building types such as steel structures, historical masonry structures, and industrial facilities [10–17]. The Antakya district in Hatay Province was one of the regions that experienced the most severe impacts of the February 6 earthquakes. This area, characterized by a building stock with diverse features in terms of construction year and number of stories, experienced significant damage during the first earthquake (the Mw 7.8 Pazarcık earthquake). Many

* Corresponding author.
E-mail address: gani20@itu.edu.tr (E. Gani).

https://doi.org/10.1016/j.soildyn.2025.109608
Received 27 January 2025; Received in revised form 10 June 2025; Accepted 10 June 2025
Available online 28 June 2025

buildings, whether they had received professional engineering services, failed to achieve the seismic performance levels required for life safety, suffering heavy damage or partial to total collapse. The causes of the widespread destruction and damage in the region include various factors such as unethical construction practices, workmanship errors, unregulated construction, insufficient inspection, and design deficiencies. Furthermore, the effects of near-fault phenomena, multi-segment rupture, and the transfer of extraordinary seismic energy due to local soil conditions during the February 6 earthquakes likely contributed significantly to the observed outcomes.

One of the most significant characteristics of the ground motion records from the Pazarcık earthquake is the presence of velocity pulses, particularly identified at near-fault stations. This phenomenon indicates the influence of forward directivity and fling effects, for which the Antakya region is well-suited due to its position relative to the fault and the rupture propagation direction. Chen [18] analyzed records from stations that captured the February 6 earthquakes, identifying pulse-like ground motions and highlighting their greater damage potential compared to ordinary ground motions. Similarly, Baltzopoulos et al. [1] characterized the pulse-like features of ground motions in their study. Chang et al. [19] further distinguished between directivity and fling effects by associating permanent ground displacements with fling effects, enhancing the characterization of these records. Wu et al. [20] used wavelet analysis to examine the identification and effects of velocity pulses. Their study investigated how the earthquake's focal and rupture mechanisms influence the orientation and amplitude of velocity pulses and how these characteristics affect the response spectrum. Additionally, Ertuncay and Costa [21] and Hu et al. [22] focused on impulsive ground motions, reporting that the vertical acceleration components at certain stations exceeded the horizontal ones and that the peak ground velocity (PGV) values were significantly higher than those predicted by ground motion prediction equations. They also noted that high-period, high-amplitude signals indicate directivity effects.

On the other hand, the mainshock occurred along a previously unmapped fault segment [23]. Subsequent research has revealed that the rupture velocity during the second earthquake reached supershear speeds, with some studies suggesting similar phenomena for the first earthquake as well [24,25]. Furthermore, it has been argued in the literature that this supershear rupture triggered multi-segment ruptures in the region [26]. Supershear ruptures generate intense ground motions and largely unattenuated shock waves, which can amplify the magnitude and extent of structural or ground failures. In particular, within the supershear propagation zones to the south, it has been observed that slip rates exhibited rapid changes over short distances. This unstable supershear propagation likely intensified the shaking and enhanced the energy release [20]. The supershear ruptures identified in previous studies are likely to have played a significant role in exacerbating the severe damage and destruction observed in the Antakya region. The complex fault network in the Antakya area complicates the detection of the potential effects of supershear phenomena in the region. However, detailed analyses of station records reveal traces of these effects, further underscoring their contribution to the observed damage.

Some studies in the literature suggest that, in addition to the aforementioned factors, basin effects also contributed to the severity of the destruction in Antakya [27–29]. Antakya is predominantly characterized by soft soils, which are believed to amplify the ground motion during an earthquake. Furthermore, Hatay province generally consists of numerous villages and towns situated in sedimentary basins surrounded by mountains. This geographic configuration may result in the trapping of seismic waves within the sedimentary basin, leading to the accumulation of energy and subsequently causing larger ground motions on the surface. Additionally, Duan et al. [2] have proposed that the characteristic features of the vertical acceleration values observed in station records point to a trampoline effect. The trampoline effect is a phenomenon proposed after the 2008 Iwate Miyagi Inland (Japan) earthquake. It explains the asymmetric amplification of vertical ground accelerations for both positive and negative values, which is caused by the nonlinear vertical behavior of the soil [30].

Analyses based on strong ground motion station records have shown that the primary cause of the severe destruction in the Antakya region was the first Mw 7.8 Pazarcık earthquake [27]. The second earthquake, the Mw 7.6 Elbistan event, also played a role by increasing the plastic deformation demands on buildings that were already damaged or had approached the limit of their stability during the first earthquake, which led to additional damage or collapse through a cumulative effect. Several researchers have emphasized that the horizontal and vertical spectral acceleration values recorded during the Pazarcık earthquake exceeded the DD2-level (return period of 475 years) elastic design spectrum values prescribed by Turkish Building Earthquake Code 2018 (TBEC 2018) [31] for the corresponding station locations, and at certain stations, even surpassed the DD1-level (return period of 2475 years) elastic design spectrum accelerations [1,13,32]. In near-fault locations, it has been previously reported that design spectral acceleration values are sometimes predicted lower than the recorded ground motion spectral values. Iervolino et al. [33] indicated that the acceleration spectra of pulse-like ground motion records, which result from directivity effects, have the potential to exceed design spectra. In such cases, the inelastic displacement demands imposed by seismic motion on structures may be higher compared to those caused by non-pulse-like records. Iervolino et al. [34] also emphasized that strong earthquakes occurring near faults are more likely to produce ground motions that exceed the design spectra. Design spectra are typically developed based on a specified exceedance probability, an appropriate selection of earthquake records, and probabilistic seismic hazard assessment methodologies. When phenomena such as directivity, fling, basin and trampoline effects, supershear ruptures, and multi-segment faulting are present, it is not unexpected for ground motions to exceed the design spectra, especially if these effects are not explicitly considered in the probabilistic framework. Thus, the exceedance of design spectra under near-fault effects is not an extremely rare situation. On the other hand, it is essential to characterize the causes of design spectra exceedances, since the structural safety of newly designed buildings will depend on the safety margins provided by their inelastic behavior once the design spectra are surpassed. Similarly, considering that the TBEC2018 DD2 elastic design acceleration spectra are used in the seismic performance assessment or retrofitting of existing residential buildings, the safety of life and property in these structures would be at significant risk if they are exposed to seismic demands that exceed the anticipated levels. As a result, the exceedance of design acceleration spectra by the acceleration spectra of recorded signals in Antakya provides important indications of the influence of near-fault and site-specific effects. These effects played a significant role in amplifying the extent of damage and destruction observed in the area. In other words, if the station-recorded acceleration spectra had been at levels similar to the TBEC-2018 design spectra, the extent of damage and collapse would likely have been lower than what was actually observed. This is because many buildings in the region, particularly those constructed after 2007, were designed based on spectral accelerations significantly lower than those recorded during the Pazarcık earthquake. Therefore, examining the role of mechanisms such as supershear ruptures, pulse-like ground motion and site amplifications within the standard design process, and incorporating these effects into design procedures when necessary, is of great importance for both structural engineering practice and life safety. Another important point is that the severe damage and destruction observed in Antakya should not be attributed solely to the exceedance of acceleration spectra. The seismic demand experienced by buildings depends on both the fundamental periods of the structure and the soil. Thus, a two-story building would not be affected by spectral acceleration peaks occurring at a period of 2.5 s due to the directivity effect.

In studies on the Pazarcık earthquake, researchers have mostly focused on one or two effects, such as supershear rupture, directivity, or site amplification. However, these studies have consistently shown that

none of these phenomena alone can fully explain the ground motion characteristics observed in the Antakya region. This highlights the need to explore scenarios where multiple ground motion effects and site-specific conditions interact, and to assess how this combination influences the complexity of the recorded signals. In this study, ground motion records from seven different seismic stations located in the Antakya region were analyzed in detail. The characteristics of both the recorded motions and the derived spectral responses were examined, and the potential causes behind these observations were discussed to clarify the nature of the ground motions and the recorded data. Following this, the severe damage and destruction observed in the Antakya region were evaluated, and the potential role of the identified phenomena in the catastrophic outcomes caused by the earthquake was discussed. The findings on building damage and collapse presented in this discussion are based on regional damage observations rather than building-specific data. In other words, due to the lack of detailed damage information at the building level that would allow a direct correlation between the recorded ground motions and the damage observed in individual structures, the conclusions in this study are drawn from general building characteristics and regional damage patterns. More accurate insights could be obtained through seismic performance evaluations by conducting building-specific nonlinear analyses.

2. Potential factors increasing seismic effects in Antakya

Antakya is the largest district in Hatay Province, covering 12.7 % of the total area and hosting 298,620 residents, which accounts for 19.3 % of the province's population as of 2023 [35]. The district is bordered by the Habib-i Neccar Mountain, forming a natural southwest-northeast boundary, while the Asi River flows through its center. Within the context of Hatay Province, Antakya sustained the most significant impact from the Mw 7.8 Pazarcik earthquake. This conclusion, visually evident, is further supported by numerical data from damage assessment studies conducted by the Ministry of Environment, Urbanization, and Climate Change. Following the earthquake, the Ministry categorized buildings into six damage states based on field observations, which were published on its website along with district and neighborhood-level address data [36]. Although these data are not officially certified, they provide valuable insights into the extent of damage and destruction. By aggregating the Ministry's data, the damage status of buildings at the district level has been determined and is presented in Table 1.

The Antakya region experienced the most severe damage and destruction caused by the February 6th earthquakes. As shown in Table 1, the combined percentages of damage types D, E, and F are highest in Antakya (46 %), followed by Defne (36 %), Kırıkhan (29 %), Hassa (27 %), and Samandağ (26 %). Buildings classified as type E are those rendered unusable due to collapse, including partial collapses. Therefore, when type E and F buildings are considered as collapsed structures, Fig. 1a clearly demonstrates that Antakya suffered significantly more destruction than other districts. Similarly, Fig. 1b shows that Antakya and its neighboring district, Defne, have the highest percentages of heavily damaged buildings, excluding collapsed ones.

2.1. Directivity and fling effect in Antakya

The identification of velocity pulses is the most prominent indicator of directivity and fling effects. In strike-slip events, directivity is characterized by velocity pulses in the fault-normal direction, while fling effects are associated with velocity pulses in the fault-parallel direction. The key distinction between these effects is that fling effects involve permanent ground displacement, whereas no such displacement occurs in directivity [37]. Various researchers have analyzed ground motion records from stations to identify velocity pulses (Table 2). These analyses provide characteristic parameters, such as azimuths, which define pulse orientations, and pulse periods (Tp). The azimuths in Table 2 are measured as positive angles counterclockwise from the eastward global axis. Due to differences in pulse detection methods and the assumptions underlying these approaches, the results reported by different studies vary.

Wu et al. [20] and Baltzopoulos et al. [1] employed the method proposed by Baker [38] for velocity pulse detection. In this method, the velocity time-history components are rotated at 1-degree intervals up to 180°, and a wavelet-based approach is applied to identify candidate pulses, resulting in the calculation of Pulse Index (PI) values. Based on the PI value, it is determined whether the signal is pulse-like, and additional parameters such as pulse orientation and pulse period can be extracted. In Wu et al. [20], three criteria were considered for defining a record as pulse-like: (1) a Pulse Index greater than 0.85, (2) the extracted velocity pulse record achieving 10 % of the total energy before the original signal reaches 20 % of its total energy, and (3) a PGV value greater than 30 cm/s for the original velocity signal. In contrast, Baltzopoulos et al. [1] defined records as pulse-like if the Pulse Index exceeded 0.90. In Hu et al. [22], pulse-like ground motions were identified using the Shahi and Baker [39] method. Chang et al. [19]

Table 1
Damage assessments provided by the Ministry for Hatay Province [36].

Hatay Districts	Total Number of Buildings	Damage statuses for each district (%)					
		Undamaged	Slightly Damaged	Moderately Damaged	Severely Damaged	Immediate Demolition	Collapsed
Antakya	63428	15.43 %	32.78 %	5.38 %	29.42 %	6.95 %	10.04 %
Defne	25272	20.68 %	36.50 %	6.94 %	27.97 %	4.02 %	3.89 %
Belen	9808	61.82 %	27.13 %	1.60 %	7.31 %	0.73 %	1.41 %
Iskenderun	36904	35.70 %	50.67 %	3.03 %	8.40 %	0.94 %	1.27 %
Arsuz	29460	58.05 %	32.07 %	2.74 %	5.87 %	0.65 %	0.62 %
Dötyol	25195	58.19 %	32.53 %	2.54 %	6.05 %	0.26 %	0.42 %
Erzin	12472	68.35 %	26.07 %	1.14 %	4.37 %	0.03 %	0.05 %
Hassa	15321	39.19 %	31.75 %	2.02 %	16.67 %	3.64 %	6.72 %
Kırıkhan	27756	28.70 %	38.32 %	4.04 %	20.28 %	2.07 %	6.59 %
Kumlu	4114	52.67 %	25.28 %	1.17 %	15.97 %	1.80 %	3.11 %
Payas	8129	52.66 %	39.14 %	1.59 %	5.51 %	0.47 %	0.63 %
Reyhanlı	22948	65.36 %	24.42 %	1.61 %	6.72 %	0.51 %	1.39 %
Samandağ	26285	31.00 %	35.95 %	6.61 %	21.48 %	2.34 %	2.62 %
Yayladağı	11701	68.13 %	15.66 %	2.34 %	11.01 %	1.10 %	1.76 %

Undamaged (A): Buildings with no damage.
Slightly Damaged (B): Buildings with minor cracks in paint, plaster, or walls, and plaster detachment.
Moderately Damaged (C): Buildings with wall cracks and minor cracks in load-bearing elements.
Severely Damaged (D): Buildings with extensive and widespread shear cracks or separations in load-bearing elements.
Immediate Demolition (E): Buildings where load-bearing elements have undergone significant residual displacement, leading to partial or complete collapse.
Collapsed (F): Situations involving total collapse beyond the state of immediate demolition.

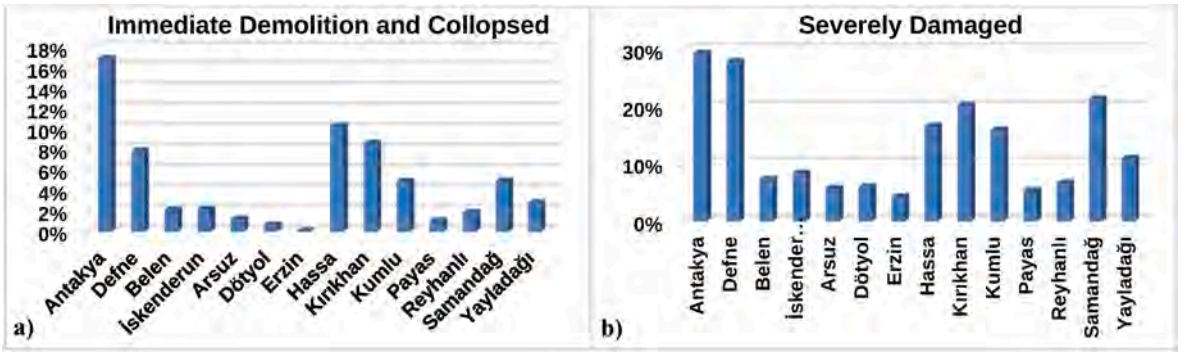

Fig. 1. a) Immediate Demolition + Collapsed and, b) Severely Damaged building percentages for each district in Hatay.

Table 2
Pulse-like ground motion identification by different researchers.

Station Data			Wu et al. [20]		Hu et al. [22]		Baltzopoulos et al. [1]		Chang et al. [19]	
ID	$V_{s,30}$ (m/s)	Latitude/Longitude	Azimuth (°)	Tp (sec)	Azimuth (°)	Tp (sec)	Azimuth (°)	Tp (sec)	Azimuth (°)	Tp (sec)
3123	470	36.21423/36.15973	90	2.5	71	2.62	68	2.62	70	2.1
3124	283	36.2387/36.1722	109	3.4	100	3.57	–	–	100	2.9
3125	448	36.23808/36.13264	–	–	135	3.42	117	3.43	90	3.1
3126	350	36.2202/36.1375	–	–	158	3.37	112	3.28	–	–
3129	447	36.19117/36.1343	–	–	81	1.76	90	1.75	90	1.4
3131	567	36.19121/36.16328	–	–	155	12.3	–	–	110	7.7
3132	377	36.20673/36.17159	–	–	–	–	–	–	–	–

introduced a newer method for pulse-like detection, referred to as the Chang et al. [40] method, which uses the Gabor wavelet algorithm [41]. This approach filters out low frequencies from the original signal, resulting in a smoothed ground motion. Candidate pulses are then fitted indirectly in both time and spectral domains using the smoothed ground motion. In this method, the Energy of Velocity Pulse (EVP) parameter is defined, and signals with an EVP value greater than 0.35 are classified as pulse-like. In Table 2, it is important to interpret the differences in reported azimuths with caution, as they can be misleading. While it is useful to indicate the direction of the pulse-like component of ground motion, such motions usually keep their pulse-like nature across a wide range of angles around that main direction. Also, care should be taken when defining the pulse period (Tp). In general, Tp values greater than 10 s may be the result of using double-sided wavelets to represent pulses that are actually one-sided. For example, at station 3131, a 12.26-s pulse is reported using a 4th-order Daubechies wavelet [22]. However, Baltzopoulos et al. [1] does not report this pulse because the mismatch in the pseudo-velocity spectra suggests that Tp was overestimated due to this issue. On the other hand, Chang et al. [19] reports a much shorter pulse—about half the duration—because it uses single-sided fling-step pulses, which may give a more accurate result in this case. However, it should be noted that, regardless of the different approaches applied in identifying pulse orientations and pulse periods, these results provide valuable insights into the pulse-like characterization of the ground motion. Both Wu et al. [20] and Baltzopoulos et al. [1] associated velocity pulses with rupture directivity or fling effects but did not perform numerical characterization of the identified pulses in this context. Wu et al. [20] linked the pulses observed in records located more than 20 km from the fault to forward directivity effects, while pulses in records closer than 20 km, especially those within 5 km, were associated with fling-step effects. Chang et al. [19] analyzed whether ground motions caused permanent displacement and categorized pulse-like ground motions with permanent displacement as fling effects, while others were categorized as forward directivity. However, the study emphasized that permanent displacements could be influenced by extraneous movements of recording equipment or noise from the sensor's electrical or mechanical properties. Therefore, it was stated that permanent displacement data must be verified with geodetic measurements before being considered definitive, and such categorizations should be regarded as preliminary analyses. Based on this preliminary analysis, pulses at stations 3124 and 3125 were attributed to forward directivity, while those at stations 3123, 3129, and 3131 were attributed to fling effects. Contrary to Table 2, other studies in literature report different findings regarding pulse detection. For instance, Guan Chen [18] identified a pulse at station 3132, while no pulses were detected at stations 3125, 3126, or 3129. Similarly, Ertuncay and Costa [21] observed pulses only in the vertical component at stations 3124 and 3125, with no pulse effects identified in any component at stations 3126 and 3129. This complex scenario arises not only from the differences in the methods employed but also from the intricate nature of ground motions that encompass multiple phenomena. The observed complexity can be attributed to the potential interplay of various factors, including the segmented and intricate tectonics of the fault, multi-segment ruptures and cumulative wave propagation of energy, and ground behavior influenced by geological and geographical characteristics.

2.2. *Asperities and supershear in Antakya*

In seismology, a supershear earthquake occurs when the rupture propagation speed along the fault surface exceeds the shear wave (S-wave) velocity [42]. During the February 6 Kahramanmaraş earthquakes, the mainshock occurred on the previously unmapped Narlı-Pazarcık Fault (NPF), rather than directly on the East Anatolian Fault (EAF). The rupture extended approximately 350 km, while the second earthquake, triggered 9 h later, ruptured about 160 km along the Sürgü Fault [26]. For the Mw 7.8 earthquake, the maximum rupture speed was calculated as 3.2 km/s. In the Mw 7.6 earthquake, rupture speeds of 4.8 km/s to the west and 2.8 km/s to the east were recorded. The maximum displacements for the two earthquakes were estimated at 8 m and 6 m, respectively [23]. The slip was segmented between the branch parallel to the EAF and the portion extending to the intersection of the Sürgü Fault with the EAF. Slip initiation on the EAF was delayed until the rupture front from the NPF reached the intersection point, after which bilateral propagation occurred. Kinematic inversion analysis indicated

that the best fit to the data was achieved with a rupture speed of 3.2 km/s. Fig. 2 illustrates the southwest and northeast propagation of the first earthquake at 45.25 s after the onset of the event along the NPF. The second earthquake initiated on the Sürgü Fault, propagated bilaterally, and diminished as it approached the fault's two ends [23].

It has been emphasized that, particularly during the second earthquake, a single rupture velocity value did not yield accurate results in modeling studies. Instead, the rupture propagated at supershear velocity toward the west and at sub-shear velocity toward the east. However, conclusive evidence of a definitive supershear rupture during the first earthquake remains lacking. Based on strong ground motion records, Rosakis et al. [25] argued that a supershear rupture must have occurred at the onset of the first earthquake, whereas Melgar et al. [23] suggested that this was not necessary. Nonetheless, Melgar et al. [23] acknowledged the possibility of an initial supershear rupture, which may have transitioned to sub-shear velocities, making it less apparent in ground motion records due to their reliance on long-period waveforms. Rosakis et al. [25] highlighted that the dominance of the fault-parallel velocity component over the fault-normal component is a distinguishing feature of supershear ruptures exceeding the shear wave velocity of crustal material. This behavior was observed at the NAR recording station. Additionally, subshear velocities were initially recorded at the near-fault 4615 station during the first earthquake, but the rupture later transitioned to supershear speeds. This early supershear transition, coupled with the weak attenuation of Mach fronts over distance, may have facilitated strong dynamic stress transfer along the East Anatolian Fault (EAF), potentially triggering rupture propagation and slip in both the northeastern and southwestern directions, affecting regions such as Hatay. Ren et al. [43] reported supershear ruptures on the splay fault during the first event, as well as on the Pazarcık and Erkenek segments, while subshear ruptures were observed on the Amanos segment in the southwest. They emphasized the critical role of supershear rupture in triggering multi-segment ruptures during the 2023 Kahramanmaraş twin earthquakes. However, many studies have highlighted the complexity of the rupture characteristics of the first earthquake, involving the Amanos, Pazarcık, and Erkenek segments, making seismic behavior particularly challenging to predict. Towhata et al. [44] analyzed the strong ground motion in the Antakya region, focusing on variables such as longer dominant periods and shorter durations, in the context of supershear mechanisms. Their study emphasized that rupture propagation speeds exceeding 3 km/s across multiple fault segments in the region could be associated with supershear mechanisms [45,46]. The study reproduced spatial variations, such as stronger shaking and shorter durations, under supershear conditions. It was noted that supershear ruptures generate Mach wavefronts due to rupture speeds exceeding the S-wave velocity of the medium, leading to concentrated

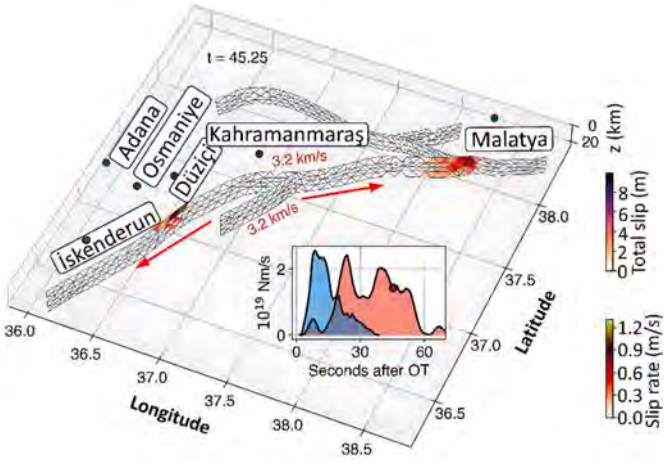

Fig. 2. Rupture propagation at 45.25 s of the first earthquake [23].

wave energy and intense ground motion. Modern seismology suggests that wave propagation initiated by a small strike-slip fault displacement is equivalent to stress application triggered by a double-couple model in an elastic medium [47–49]. In this context, analyses comparing scenarios with and without supershear ruptures revealed that energy concentration and wave development are significantly more intense under supershear conditions, resulting in stronger vibrations and shorter wave development times. The study concluded that this phenomenon, associated with Mach wavefronts, played a significant role in the stronger shaking observed in Antakya and surrounding regions. Abdelmeguid et al. [24] analyzed accelerometer recordings from stations in the earthquake-affected region. Using findings from Rosakis et al. [25] and Mello et al. [50], which associate the dominance of fault-parallel velocity components with supershear rupture, stations were categorized into three groups: sub-Rayleigh, potential supershear, and supershear. Stations 2712, 3143, and 3137 were classified as sub-Rayleigh due to dominant fault-normal velocity components, while stations 3123, 3124, 3129, and 3145 were identified as supershear, where fault-parallel velocity components indicated rupture propagation at supershear speeds.

In the Kahramanmaraş earthquakes, asperities—relatively stronger and structurally resistant areas on the fault plane—were observed. These asperities arise from physical heterogeneity, fault geometry complexities, or high-friction zones and significantly influence the earthquake's characteristics. During the February 6th earthquakes, four major asperities and two smaller slip regions were identified, where energy release was concentrated along the fault. The dynamic interaction between these asperities and the "jumping rupture" mechanism explains the complex rupture behavior and large surface deformations observed [43,51,52]. Following the mainshock, destruction propagated northeastward at supershear speeds and spread to the Antakya region at subshear speeds. In this complex region, involving multiple fault segments, supershear rupture was triggered remotely. The resulting supershear wave reflected and combined with the incoming subshear rupture, creating a unique propagation model. Intense ground motion and shock waves from supershear ruptures, which attenuate minimally, amplified the extent of damage, particularly in the southern regions. Rapid changes in slip rate over short distances, exceeding 50 % within 5–10 km, were observed in supershear propagation zones (Fig. 3a). These variations, referred to as "rapid change," are directly linked to velocity pulses recorded in these regions, where rupture speeds exceed the shear wave velocity. Such spatial heterogeneity in the rupture process amplifies ground motion intensity and radiated energy, imposing higher demands on structures. Narrow velocity pulses, as observed in Antakya, increase the likelihood of structural collapse. Abdelmeguid et al. highlighted that, except for station 3125, the FP/FN (fault-parallel to fault-normal) component ratio was dominant in other stations across Hatay. However, the study noted that the region's complex fault geometry, with multiple bends and branching segments, created intricate stress conditions. These conditions likely caused supershear velocity bursts in some segments while generating complex wavefronts that could obscure Mach cone signatures in others. This phenomenon may have led to stress shadowing in certain segments, reducing rupture speed and halting propagation. Dynamic modeling analyses revealed a strong correlation between spatial variations in rupture speed along the fault and the FP_{max}/FN_{max} ratio. As shown in Fig. 3b, when the rupture speed (Vr) exceeds the shear wave velocity (Cs), the FP/FN ratio surpasses 1. Additionally, in supershear mechanisms, as rupture speed increases, the strengthening of the FP component due to Mach cone passage further elevates the FP/FN ratio.

In the Hatay region, the complexity and intensity of wave fields were noted to increase due to the highly segmented structure of the East Anatolian Fault (EAF). It was observed that sub-Rayleigh ruptures interacting with fault branches triggered supershear bursts, resulting in a region dominated by complex ground motions associated with multiple propagating Mach cones. Numerical modeling confirmed the consistency of this observation. This finding aligns with ground motion

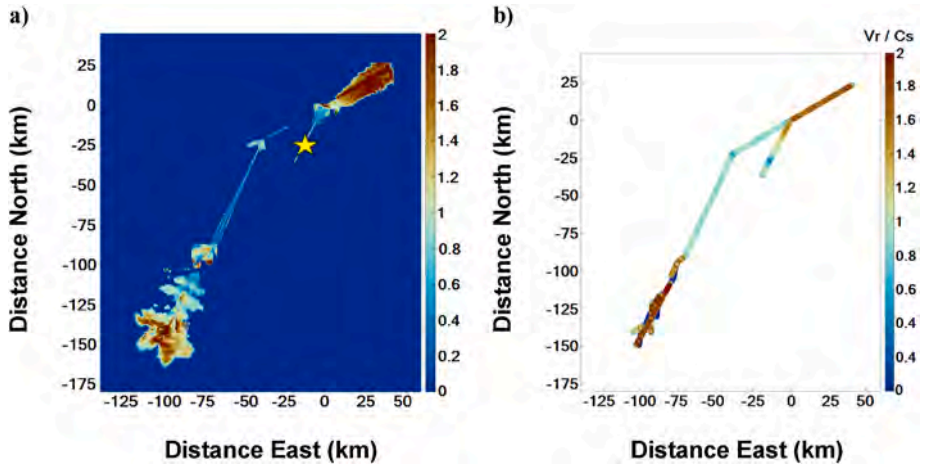

Fig. 3. a) The spatial distribution of the FP to FN velocity jump ratios computed from the numerical model, b) 2D plot showing rupture speed variation within the dynamic rupture model [24].

records, which revealed dominant fault-parallel (FP) and fault-normal (FN) components in the southern regions, as well as with the widespread damage and destruction observed in these areas. Additionally, Xu et al. [53] conducted waveform correlation analyses on the southwestern segment but did not detect a persistent Mach cone signature in the far field. However, such correlations were linked to long-distance supershear rupture propagation. The episodic supershear propagations described in this study further highlight the unstable nature of supershear ruptures, which amplify shaking intensity and strengthen the energy being radiated. Ground motion records from stations 3123 and 3129 in Antakya revealed a relatively narrow (1–2 s) dominant pulse in supershear propagation regions, distinct from the broader pulses observed in sub-Rayleigh propagation. This feature, also emphasized by Wu et al. [20], imposes higher demands on structures and increases the likelihood of structural collapse. Numerical analyses further suggested that stress and friction conditions along the fault are heterogeneous, contributing to the continuous propagation of the rupture and influencing rupture velocity. Moreover, several fault segments are highly stretched due to their orientations relative to the tectonic stress field. For instance, this condition facilitated the early supershear transition on the Narlı Fault and the supershear propagation pulses observed in the southern regions.

2.3. Basin effects in Antakya

Basin effects refer to the trapping of seismic waves within a large sedimentary basin, where the geometric structure of the basin causes accumulated energy to amplify ground shaking at the surface. This phenomenon occurs as seismic waves are reflected from the basin edges and accumulate in the interior. The shape and size of the basin influence the amplitude and frequency of the waves, with significant effects observed in large, expansive areas. Basin effects have been documented in past earthquakes, including those in Caracas (1967), Michoacan (1985), Peru (1974), Armenia (1988), Loma Prieta (1989), Gorkha (2015), and Samos (2020) [27]. In Antakya, the potential for seismic intensity amplification due to soft soil characteristics has been highlighted in previous studies [54,55]. During the February 6th earthquakes, basin effects were reported in the region. According to Karray et al. [27], sedimentary basins and valleys bounded by rigid materials exhibit complex two-dimensional (2D) and three-dimensional (3D) amplification phenomena. The study noted very high spectral acceleration values of 0.3s in Hatay, located 150 km from the epicenter, and 1s spectral acceleration values in Hassa, 75 km away, emphasizing the role of basin effects in these observations.

Antakya, the central region of Hatay, is situated on alluvium covering the Dead Sea Fault and near the Taurus Mountains, extending toward the Dead Sea. The city lies on the Hatay Graben, a rift valley formed by tectonic forces. High acceleration values (Sa(0.3s) ≈ 4g) were detected in sedimentary basins during the earthquake. Karray et al. [27] investigated the role of soil amplification in these high PGA and spectral acceleration values. Amplification was defined as the ratio of acceleration values between rock and softer soils. For this analysis, acceleration spectra from station 3129 and corresponding TBEC-2018 DD1 design spectra were obtained. Additionally, spectra for station 3116 were plotted, but a direct comparison with station 3129 was avoided due to significant differences in their distances from the fault. Instead, spectral values for Rjb = 10 km were calculated using attenuation relationships, and ratios for PGA, 0.3s, and 1s periods were determined as 3, 4–4.5, and 3.5–4, respectively, indicating amplification during transitions from rock to softer soils. Significant amplifications were also observed at 2s periods, suggesting that the sedimentary basin in Antakya is thick and rigid. Işık [28] identified basin effects based on velocity-time and displacement-time data from station 3124, where earthquake data exceeded the regulatory acceleration spectrum at higher periods. Similarly, İlhan et al. [29] noted that spectral acceleration values predicted through one-dimensional nonlinear and equivalent-linear ground response analyses for station 3139 in Hassa were lower than the recorded values, which could also be attributed to basin effects. Given that Hatay province consists largely of towns and villages surrounded by sedimentary basins and mountains, basin effects are considered a significant factor contributing to the severe damage in the region. The ground motion recording stations in Antakya and the region's topographic features are shown in Fig. 4.

3. Analysis of ground motion records

A detailed examination of the seismic stations located in the Antakya region reveals significant indications of the presence of forward directivity, fling, supershear, and basin effects. Ground Motion Prediction Equations (GMPEs) are among the effective tools for evaluating these observations. By using prediction models that are specifically developed for the tectonic and geological characteristics of the Antakya region, the estimated and recorded ground motion values can be easily compared. The discrepancies observed in these comparisons point to the aforementioned phenomena, as GMPEs are associated with probabilistically calculated standard deviations. If the ground motions are influenced by additional effects not considered in the prediction models, an increase in these deviations would be expected. Ultimately, situations where the observed deviations approach or exceed the expected thresholds can be explained by the presence of the near fault and site amplification

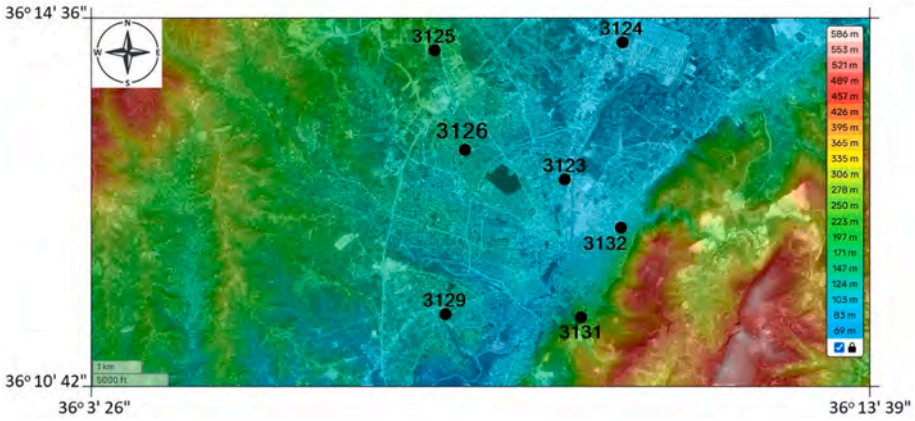

Fig. 4. Ground motion recording stations and topographic elevations of Antakya district [56].

phenomena discussed in the second chapter.

The presence of these effects can also be assessed by analyzing the spectral values obtained from the recorded data, the pulse-like characteristics of the signals, and the results of Cumulative Absolute Velocity (CAV) and Husid Plot analyses. Comparing the acceleration spectra obtained from recorded ground motions with the design spectra proposed by the current seismic code is particularly important for understanding the characteristics of the earthquake motions. The design acceleration spectra defined in the seismic code are determined by multiplying the spectral accelerations from the seismic hazard map by site coefficients, yielding elastic design spectral values for short periods, 1-s periods, and long periods. In this procedure, the spectral accelerations predicted for near-fault locations account for distance-related near-source effects. However, the specific phenomena such as

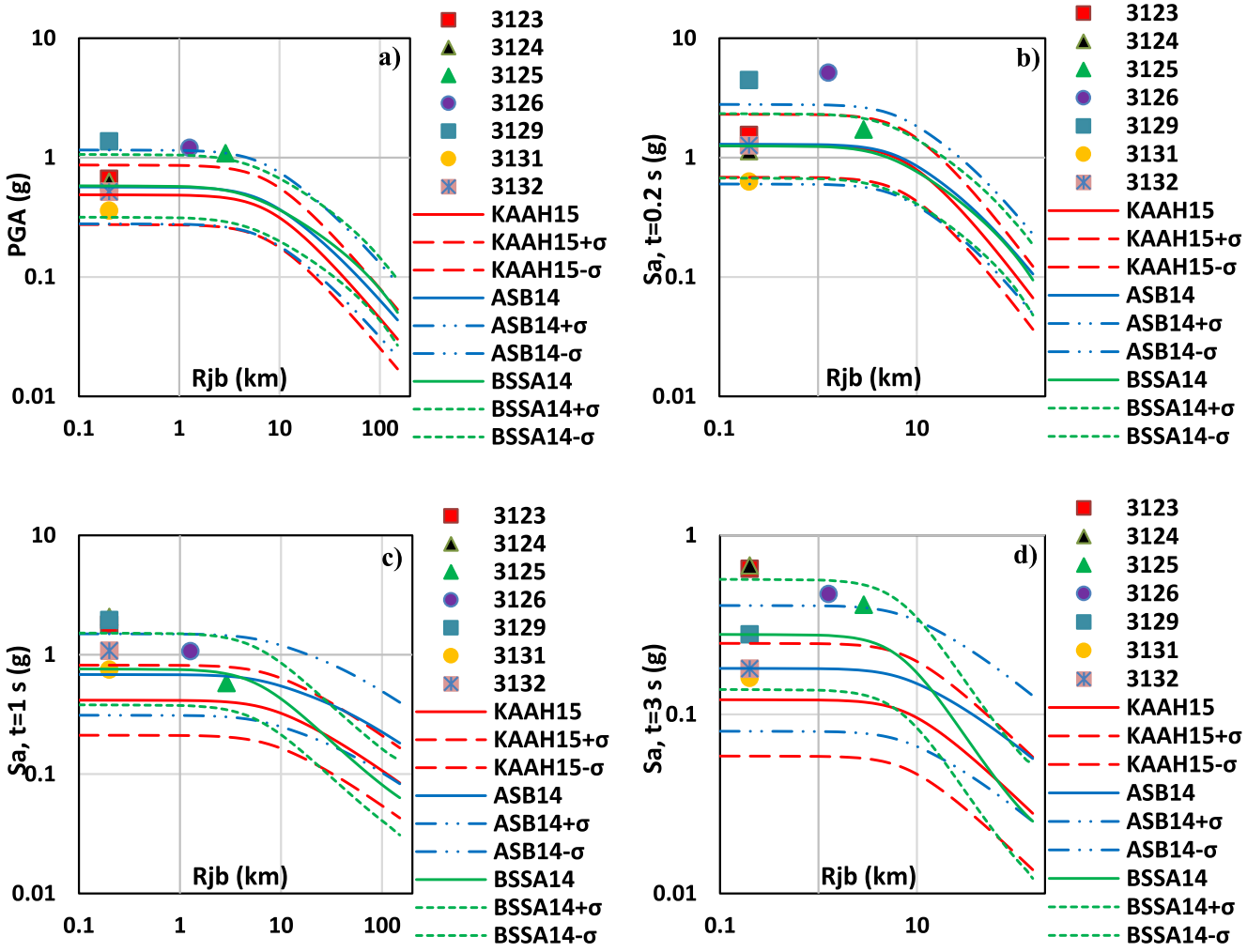

Fig. 5. Comparison of the values predicted by GMPE models and the spectral accelerations from station records at different periods: a) PGA, b) t = 0.2 s, c) t = 1 s, and d) t = 3 s.

directivity, supershear, and basin effects are not explicitly addressed through additional parameters. As a result, the discrepancies between the recorded acceleration spectra and the code-based design spectra can largely be attributed to pulse-like ground motion characteristics and site-specific effects. On the other hand, it is important to note that such a comparison involves two fundamentally different approaches. Design spectra are derived through probabilistic methods and represent a scenario-based, probability-driven approach for a given location, incorporating a range of possible events and exceedance probabilities. In contrast, the acceleration spectra obtained from ground motion records are deterministic results specific to the actual event. It is unusual for the design spectra to be much lower than the recorded spectra across many period ranges, even when considering the differences in methodology. Such discrepancies suggest the presence of effects that fall outside the predictive scope of the design spectra. Therefore, the differences observed between recorded and design spectra can be reasonably linked to the influence of these specific phenomena, supporting the conclusion that the recorded ground motions deviated significantly from standard design expectations.

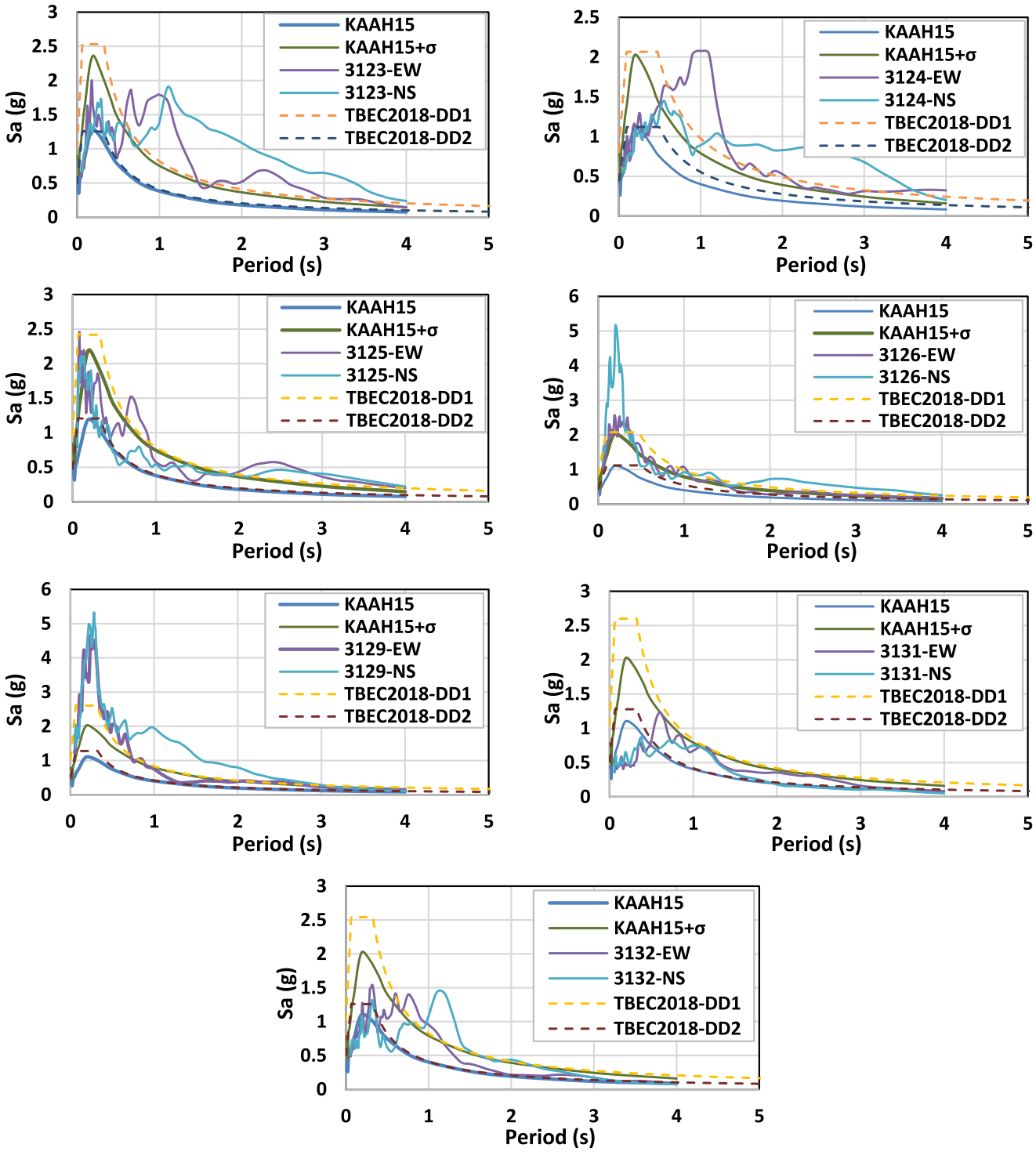

Fig. 6. Comparison of the acceleration spectra predicted by the KAAH15 model and TBEC2018 with the spectra derived from the records of Antakya stations.

3.1. Ground motion prediction equations (GMPEs)

In order to compare the results obtained from station records with prediction equations, three different prediction models were used, which are referred to as KAAH15, ASB14, and BSSA14 in the following chapters [57–59]. The values obtained from the station records were compared with the mean, mean + σ, and mean - σ predictions for each of the three models. According to the PGA comparisons, stations 3129, 3126, and 3125 exceed the standard deviation limits, while values from other stations fall within the limits (Fig. 5a). The spectral accelerations at a 0.2s period significantly exceed the upper limit at stations 3129 and 3126, while station 3125 remains near the upper limit; however, values from other stations are consistent with the model predictions (Fig. 5b). For spectral values at 1s periods, stations 3123 and 3129 exceed the limits, station 3126 approaches the upper limit, while values from other stations remain close to the mean predictions (Fig. 5c). At 3s spectral accelerations, stations 3123 and 3124 exceed the upper limit, stations 3126 and 3125 approach the upper limit, and other stations remain around the mean values (Fig. 5d). According to the results, stations 3131 and 3132 stay within the prediction limits across all periods, while other stations exhibit significant exceedances at different periods. Stations 3123 and 3124 exceed the limits at longer periods such as 1s and 3s. Stations 3126 and 3129 exceed the limits at short periods between 0 and 1 s, while station 3125 only exceeds the limit in the PGA graph, but is very close to the upper limit at the 0.2s and 3s periods. These models do not specifically incorporate phenomena such as directivity, fling, supershear, and basin effects. Therefore, the observed deviations in the models likely reflect the impact of these phenomena, both individually and in combination.

In Fig. 6, the acceleration spectra obtained from the station recordings are compared with the KAAH15 model spectra, which is considered a local model for this region and therefore more representative than the others. Additionally, the DD1 and DD2 level design spectra specified by TBEC-2018 for the respective station location are also included in the comparison. The mean and mean + σ_{max} acceleration spectra predicted by KAAH15 are generally similar to the DD2 and DD1 design spectra defined by TBEC2018, respectively. In fact, the design spectra slightly exceed the KAAH15 model predictions and fully encompass the KAAH15 spectra curves. However, the acceleration spectra of recorded signal at the stations exceed both the design spectra and the KAAH15 predictions across many period ranges. These exceedances can be attributed to the presence of pulse-like ground motion characteristics caused by phenomena such as supershear rupture, directivity, and fling effects, as well as the amplification of ground motions by the site's geological and topographic conditions. By analyzing the characteristic features of the recorded ground motions and comparing them with the design spectra, it is possible to assess and comment on the presence and influence of these effects. In the following sections of this study, the TBEC2018 elastic design spectra will be used for comparisons, as they offer a conservative and safe-side approach by also encompassing the spectra predicted by the KAAH15 model.

3.2. Characteristic properties of station ground motion records in Antakya

The original station records provided on the official website of the Disaster and Emergency Management Presidency (AFAD) [60] were first processed. Baseline correction and first-order Butterworth filter were applied to the raw data. The low and high cut-off frequencies were set at 0.025 Hz and 40 Hz, respectively. In this study, it was assumed that the records from the Antakya stations used were not affected by distortions caused by instrument offsets, thermal drift, electronic errors, or calibration issues. Accordingly, the processed ground motion records were analyzed individually, and the characteristic findings identified from the data were elaborated in detail.

3.2.1. Station 3129

The horizontal component acceleration spectra of station 3129 and the horizontal elastic design spectra recommended by TBEC 2018 [31] for the station location are presented in Fig. 7. In the EW component spectrum, the DD2 level design accelerations were exceeded at all periods. DD1 level design accelerations were exceeded by a considerable amount up to the TB corner period (Region-1), but the exceedance from the TB threshold to periods of approximately 0.9 s remained relatively low. For periods above 0.9 s, the EW component accelerations and DD1 design accelerations were generally in agreement. The spectral accelerations of the NS component showed similar characteristics to the EW component and reached quite high values until the TB period. The NS accelerations for periods longer than the TB period initially showed similar behavior to the EW component but exhibited a region where DD1 accelerations were significantly exceeded in the range from 0.7s to 2.8s (Region-2). After 2.8s, the accelerations were again in agreement with DD1 design accelerations, similar to the EW component. Two particularly notable issues arise from this analysis: (1) the very high accelerations (up to around 5g) in the plateau region of the design spectrum until the TB period, and (2) the regional high spectral accelerations of the NS component in the 0.7s–2.8s range (Fig. 7).

According to the results shown in Table 2, the maximum pulse at station 3129 occurs at azimuth angles of 80°–90°. When the original 3129 station record is rotated at 90°, the EW and NS components switch places, so the Region-2 accelerations in the NS component spectrum can be explained by the pulse effects identified in Table 2. Based on the results in Table 2, the pulse period at station 3129 ranges from 1.4s to 1.76s. The pulse effect in this period range causes the spectral accelerations in the NS component spectrum to reach high values around the pulse period. The residual acceleration spectra obtained by removing the pulse observed in the NS component are shown in Fig. 7. When the pulse effect is absent, Region-2 disappears, and a form in agreement with the EW component spectrum is obtained.

The Amanos segment fault strike is observed to form an angle of approximately 67° with the horizontal (EW component) direction (Fig. 8). This implies that the NS component of the original record is closer to the fault-parallel direction. Consequently, the Region 2 accelerations observed in the NS component indicate a fault-parallel pulse effect. According to Chang et al. [19], this pulse has been interpreted as a fling effect, which aligns well with its fault-parallel orientation and its contribution to permanent ground displacement. Abdelmeguid et al. [24] further stated that the FP/FN ratio of approximately 1.2 at this station suggests the presence of supershear.

The role of basin effects is significant in the analysis of acceleration spectra at Station 3129. Karray et al. [27] attributed the high accelerations observed in the spectra to basin effects and ground amplification. The sedimentary basin in Antakya is characterized by a thick, stiff, and dense geological structure. This composition suggests that the ground may not have sufficiently attenuated seismic effects, even at high

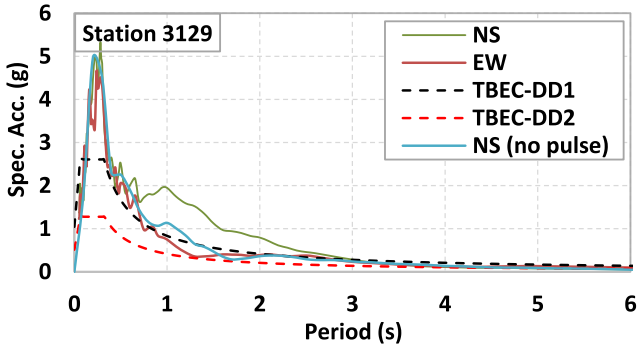

Fig. 7. Comparison of original and pulse extracted 3129 spectra with TBEC-2018 design spectra.

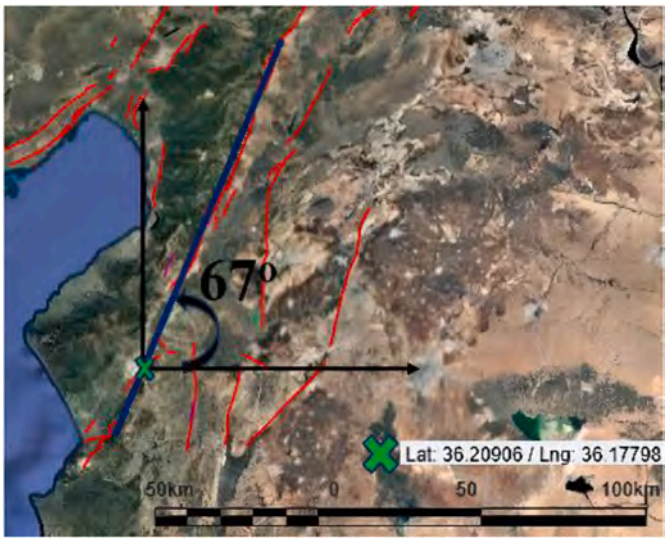

Fig. 8. The Amanos fault segment strike [61].

acceleration levels, due to its low deformation response. This behavior could lead to amplifications that exceed expected levels. Additionally, these ground amplifications might be further intensified by multiple reflections within the valley, a phenomenon that aligns with the high accelerations recorded in the spectra at Station 3129.

An important point to consider is the combined effects of basin, fling, and supershear phenomena. In the simulations discussed in Section 2, while shear wave velocities in the Antakya region are classified as subshear, the extraordinarily high accelerations at Station 3129 raise questions that cannot be fully explained by basin effects or fling alone. For instance, while basin effects are more distinctly observable at Station 3124, the magnitude of spectral acceleration amplifications observed at this location is notably lower compared to those recorded at Station 3129. Furthermore, although the fling effect explains the spectral acceleration increases near the pulse period in the NS component, it alone does not adequately account for the extremely high short-period accelerations observed in both components. This introduces the possibility of a third contributing factor: the presence of supershear effects, which could provide plausible answers to many unresolved questions. The combination of supershear effects with basin and fling phenomena emerges as a potential explanation for the extraordinarily high spectral accelerations. The potential coexistence of supershear with fling and basin effects may obscure the identification of supershear traces in velocity records using standard indicators found in the literature. Additionally, due to the complexity of fault geometry, the rupture velocity along the southeastern segment of the East Anatolian Fault (EAF) alternated between supershear and subshear, contributing to ground motions that were stronger than anticipated. Analyses have shown that the position of the EAF relative to the principal stresses places several fault segments in regions of high stress, making them highly sensitive to minor disturbances, such as dynamic stress transfers and rotations. The fault network is geometrically complex, with multiple segmentations, bends, and curvatures that significantly influence rupture propagation dynamics. This geometric complexity within the high-stress regime is thought to amplify its role in rupture dynamics through mechanisms such as the formation of high-stress concentration zones, the occurrence of arrest phases, back-propagation of earthquake ruptures, or the development of transient supershear propagation zones.

As noted in previous studies, the highly complex fault network and intricate wave propagation in the Antakya region may have significantly altered the distribution of energy and deformation. Under such conditions, it is plausible that typical supershear signatures are obscured in the records, and fault models fail to conclusively identify supershear phenomena. Following the supershear rupture identified along the splay fault [23], wave propagation directed towards the Amanos segment may have initially involved supershear rupture but subsequently transitioned into subshear speeds due to the complex fault mechanisms. This fragmented rupture likely reached Antakya's stations as a wave modulated by subshear velocities. Although most stations recorded dominant FP component jumps, the FP/FN ratios exhibited variability, which could be attributed to the region's intricate fault network. The numerous bends and branching segments at the southern end of the fault indicate a complex stress regime, possibly resulting in short-lived supershear transitions in some segments. Consequently, the records from Antakya stations may not directly capture supershear signatures but may instead reflect their combined effects with other phenomena. From this perspective, the data from Station 3129 could represent a combination of supershear-induced velocity pulses and fling effects. When amplified by basin effects, this combination might explain the exceptionally high accelerations observed at Station 3129. In such a scenario, the identification of both supershear effects and velocity pulses in velocity-time data may fall outside the scope of standard detection procedures. Supporting this notion, the records from Station 3129 were not classified as pulse-like in some studies [18,20,21].

For Station 3129, the comparison of the pulse orientation (the NS direction of the original record) with the acceleration spectra in fault-parallel directions is presented in Fig. 9a. The fault-parallel direction is derived by rotating the original record by 67°, thus corresponding to the EW acceleration spectrum. It is observed that the spectrum in the fault-parallel direction also exhibits high accelerations around 2 s, similar to the pulse orientation spectrum. This indicates that high accelerations persist even when transitioning from the pulse orientation to the fault-parallel direction, suggesting that the pulse effect is present across a broad range of orientations, including the fault-parallel direction. Considering that supershear effects are typically observed in the fault-parallel direction, this observation further supports the existence of supershear phenomena. This orientation-based inference is corroborated by the cumulative absolute velocity (CAV) results. In Fig. 9b, the EW graph represents the eastward direction (the EW component of the original record), corresponding to a 0° orientation. The highest CAV value is recorded at orientations of 60–70°, which aligns with the fault-parallel direction. Therefore, it is plausible to discuss the magnitude of energy in the fault-parallel direction and its association with supershear phenomena.

Another potential indicator of supershear phenomena is the form of the acceleration time histories. In standard acceleration records, P-waves are observed first, followed by S-waves, and subsequently by surface waves (Fig. 10a). However, in supershear earthquakes, S-waves are often not distinctly visible in the acceleration time histories [62]. For comparison, the NS component acceleration time histories of Station 3115, where supershear traces are not expected (Fig. 10b), and Station 3129, where supershear effects are believed to be present (Fig. 10c), are presented in Fig. 10. As shown, at Station 3115, S-waves can be identified prior to the surface waves. In contrast, at Station 3129, the S-wave region is absent, and sharp increases in acceleration corresponding to surface waves are observed. This phenomenon can be considered indicative of supershear occurrence.

3.2.2. Station 3124

When examining the acceleration spectra of the 3124 records, it can be observed that the acceleration values exceed the DD2 spectrum for both components. The DD1 spectrum, on the other hand, is regionally surpassed by the station's spectral accelerations. The role of basin effects in the high accelerations observed in the station 3124 spectrum is significant. The most prominent indicators of basin effects include shifting the plateau region to longer periods, creating a longer plateau, or amplifying accelerations at longer periods. These characteristics are present in the EW-NS component spectra of the original records. The plateau in the EW component acceleration spectrum resembles the

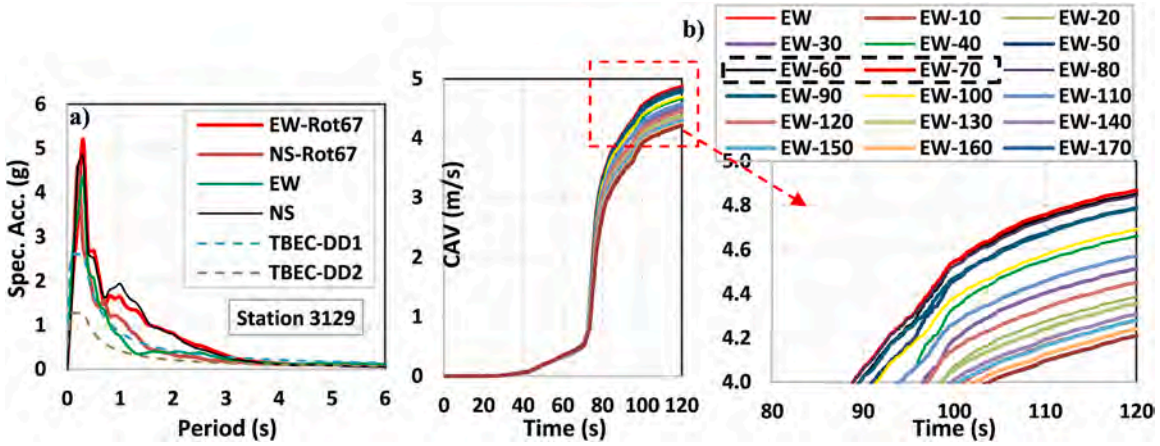

Fig. 9. a) The comparison of the pulse orientation (the NS direction of the original record) with the acceleration spectra in fault-parallel directions for Station 3129, b) CAV results.

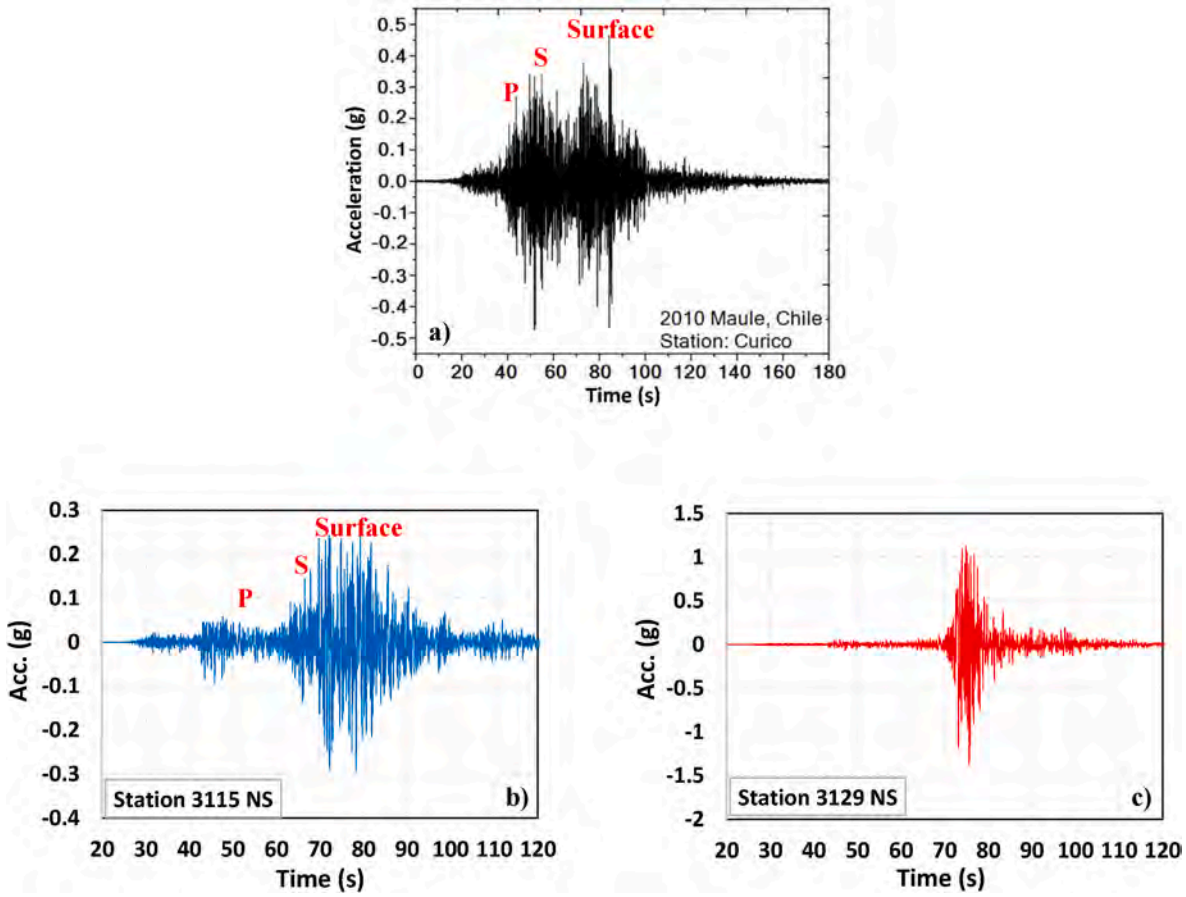

Fig. 10. Acceleration time histories for a) Typical case [63], b) Station 3115, c) Station 3129.

shifted version of the DD1 spectrum in the longer period region (Fig. 11a). In the NS component spectrum, the plateau extends and increases in acceleration at longer periods are observed. The geological and geographical structure is of great importance when investigating basin effects. The 3124 station's ground is softer compared to that of 3129. In the 3124 region, the soil may have dampened the seismic effects through its elastic-plastic behavior, and the acceleration amplifications have remained at lower levels. This is likely one of the reasons why the spectral accelerations at 3124 are not as high as those at 3129.

At Station 3124, velocity pulses were detected at azimuth angles of 100–110°, with pulse periods ranging from 2.9 to 3.4 s (Table 2). This orientation is close to the NS component, and therefore, spectral acceleration increases should be observed in the NS acceleration spectrum. As seen in Fig. 11a, the spectral accelerations in the 2–3s period range for the NS component form a peak exceeding the DD1 design accelerations. The residual acceleration spectrum, obtained by rotating the original EW component to the pulse orientation angle (100°) and removing the pulse, is shown in Fig. 11b. According to this spectrum, the accelerations around the pulse period are still very high. Therefore, the velocity pulse here is not a distinct singular pulse. Chang et al. [19] characterized this

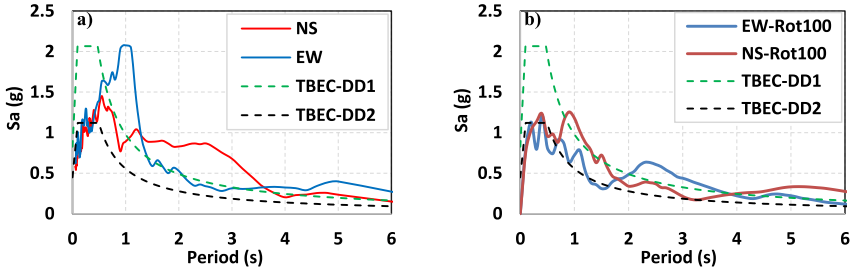

Fig. 11. a) Acceleration spectra comparison and, (b) the residual acceleration spectra for Station 3124.

pulse as a forward directivity, despite it not being aligned with the fault-normal strike, since it did not induce permanent displacement. While directivity effects are expected to manifest in the fault-normal direction, velocity pulses can also occur at different azimuth angles [64–67]. However, the presence of high accelerations in the fault-parallel direction and the shift of the pulse orientation towards the fault-parallel direction suggests the potential for a supershear effect generating velocity pulses in the fault-parallel direction. In the case of the simultaneous presence of directivity and supershear effects, it may not be possible to detect a fault-normal velocity pulse, or the pulse orientations may occur at different angles. In other words, according to Baltzopoulos [1] and Ertuncay and Costa [21], analysis of Station 3124 signals did not reveal pulse-like records. A possible fault-normal velocity pulse may be hidden due to the combined directivity-supershear effect, and the presence of such an effect may indicate the existence of other pulses in the fault-parallel direction. Furthermore, this situation can be related to the significantly higher spectral accelerations in the 0.5–1.2 s range for EW accelerations, while NS accelerations remain lower. When a fault transitions from sub-Rayleigh to supershear speed, a sub-Rayleigh signature still exists following the leading supershear rupture. This is called a trailing Rayleigh signature, which propagates at Rayleigh wave speed [50,68,69]. Consequently, a structure located near a fault will initially experience intense shaking from the shock waves of the leading supershear rupture front. This shaking occurs very quickly (and thus produces a narrow velocity pulse) and is characterized by the fault-parallel component of the ground velocity. However, a few seconds later, the structure will also be subjected to shaking primarily in the fault-normal direction, associated with the passage of the trailing Rayleigh signature. This double punch effect, related to the initial (leading) shock wave arrival and the subsequent (trailing) Rayleigh signature, may have a destructive impact on the structure.

For the examination of a potential pulse in the fault-parallel direction, the original record was rotated by 67° to obtain the EW component acceleration spectrum. As shown in Fig. 12, within the region corresponding to previously detected pulse periods, the acceleration again

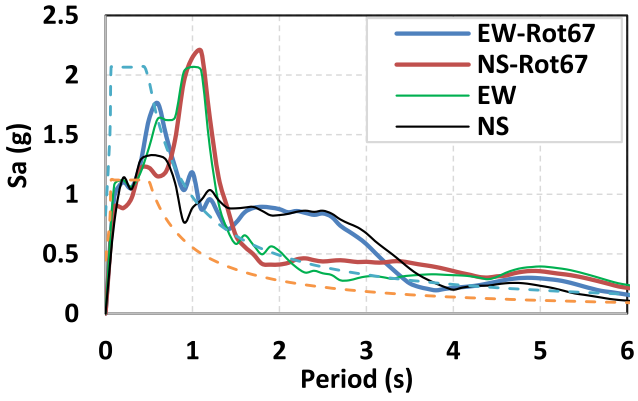

Fig. 12. Rotated acceleration spectra for Station 3124.

increases. This indicates that the effects in the fault-parallel direction are as significant as those in the pulse orientation direction, which can be interpreted as a signature of supershear.

Abdelmeguid et al. [24] have characterized the fault-parallel pulse effect at Station 3124 as a sign of supershear. Therefore, discussing the supershear effect lays the groundwork for more suitable inferences and possibilities in explaining the characteristic structures of acceleration spectra and velocity pulses. The directivity effect in the fault-normal direction, together with the supershear effects in the fault-parallel direction, may have produced a velocity pulse oriented at a 100-degree azimuth. The detection of the azimuth of the 3124 pulse as the vector sum orientation of the fault-parallel and fault-normal directions, as given in Table 2, strengthens this prediction (Fig. 13a). Fig. 13b shows the CAV values at azimuth angles of 10°. The highest CAV values at Station 3124 are reached at azimuths of 40–50°, which could also indicate high energy in the fault-parallel component.

The combined effects of forward directivity and the supershear phenomenon can also be interpreted through the varying characteristic features of the acceleration records of Station 3124 at different orientations. Fig. 14a, b and c respectively present the acceleration time histories for the 3124 EW component, the EW component rotated to the fault-parallel orientation (67°), and the velocity pulse azimuth angle (110°). As observed, secondary waves become visually indistinguishable as the orientation approaches the fault-parallel direction and the most prominent pulse angle.

3.2.3. *Station 3123*

When the acceleration spectra of Station 3123 records are compared with TBEC 2018 design spectra, similar observations to those for Station 3124 can be conducted. According to Table 2, the velocity pulse identified at this station lies within azimuth angles of 70–90°, with a pulse period ranging between 2.1 and 2.7 s. Based on the pulse orientation, significant amplification in the original NS component's acceleration spectrum is expected near the pulse period. However, the NS spectrum exhibits consistently high accelerations extending from periods above 1 s to 3.5 s, with no distinct amplification signature near the pulse period (Fig. 15a). When the EW and NS components are rotated by 67° to obtain the fault-parallel (EW') and fault-normal (NS') orientations, the acceleration spectra indicate increases near the same pulse period (Tp) in the fault-normal direction (Fig. 15b). This observation suggests the presence of pulse-like effects in the fault-normal direction, which, similar to Station 3124, could result from a combined directivity-supershear effect. The pulse signatures in the fault-normal direction may differ due to the supershear phenomenon, which is more dominant in the fault-parallel direction. The presence of this combined effect can be interpreted as the cause of high accelerations in both orthogonal directions. The velocity pulse orientation identified in Table 2 aligns with the fling effects observed by Chang et al. [19], which were indicated by permanent ground displacement. However, permanent displacement in the fault-parallel direction could also occur due to supershear effects. Abdelmeguid et al. [24] also highlighted the presence of supershear signatures at Station 3123, further supporting the supershear hypothesis. Moreover, the azimuth angles associated with the highest CAV

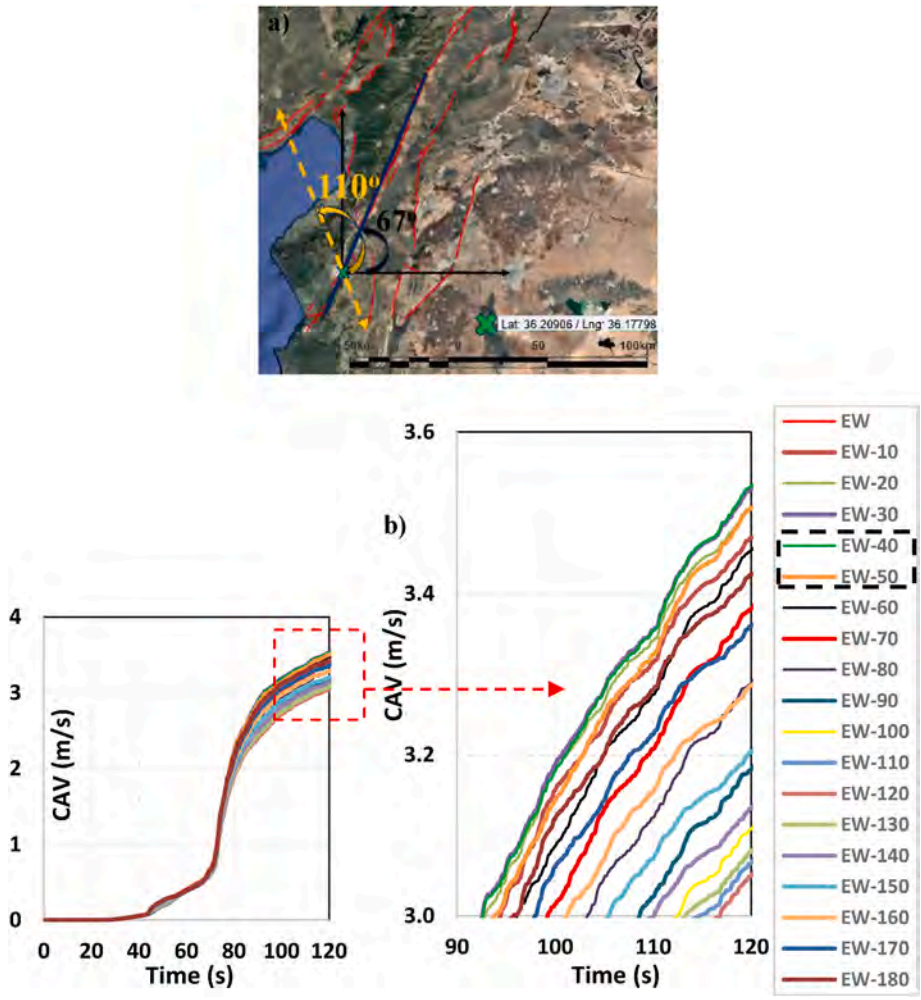

Fig. 13. a) Pulse orientation [61] and, b) CAV values at azimuth angles of 10° for station 3124.

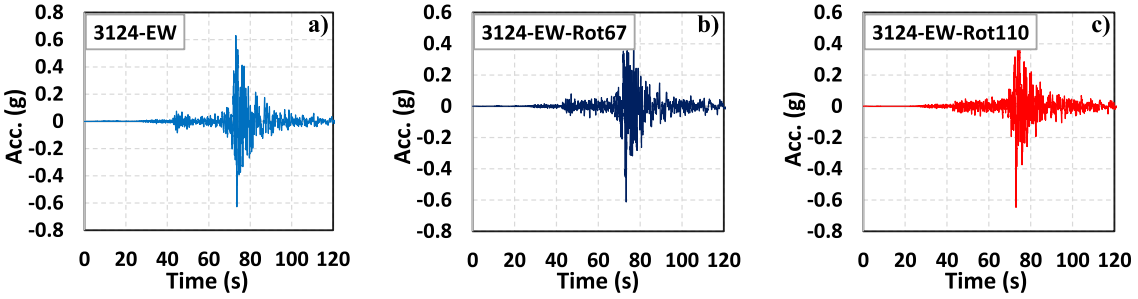

Fig. 14. Acceleration time histories for the 3124 a) EW component, b) the EW component rotated to the fault-parallel orientation (67°), and c) EW component at the velocity pulse azimuth angle (110°).

values are observed to range between 100 and 120° (Fig. 15c). These findings suggest that velocity pulses in the fault-parallel and fault-normal directions may coexist, with their resultant maximum energy appearing at an azimuth of approximately 110°.

Station 3123 is located in close proximity to Station 3124, and the basin effects described for Station 3124 are also applicable to Station 3123. Although the $V_{s,30}$ value at the station 3123 location is higher than that of 3124, basin effects should be considered on a regional scale. When the $V_{s,30}$ values are compared regionally, it becomes evident that these two stations exhibit significant similarities (Fig. 16). Additionally, the depth of the sedimentary basin in the region is substantial, and the behavior of soil layers below 30 m plays a crucial role in acceleration amplification. Therefore, drawing conclusions solely based on $V_{s,30}$ values would be inaccurate. Consequently, the plateau extensions and spectral acceleration increases in the longer period regions observed at station 3123 are indicative of the presence of basin effects at this site as well.

3.2.4. Station 3125

When the acceleration spectra of the station 3125 are compared with the TBEC 2018 design spectra, it is observed that DD2 spectral accelerations exceed the design spectra across almost all periods, while DD1 spectral accelerations exceed the design spectra within certain period ranges. Specifically, the spectral accelerations of the original EW

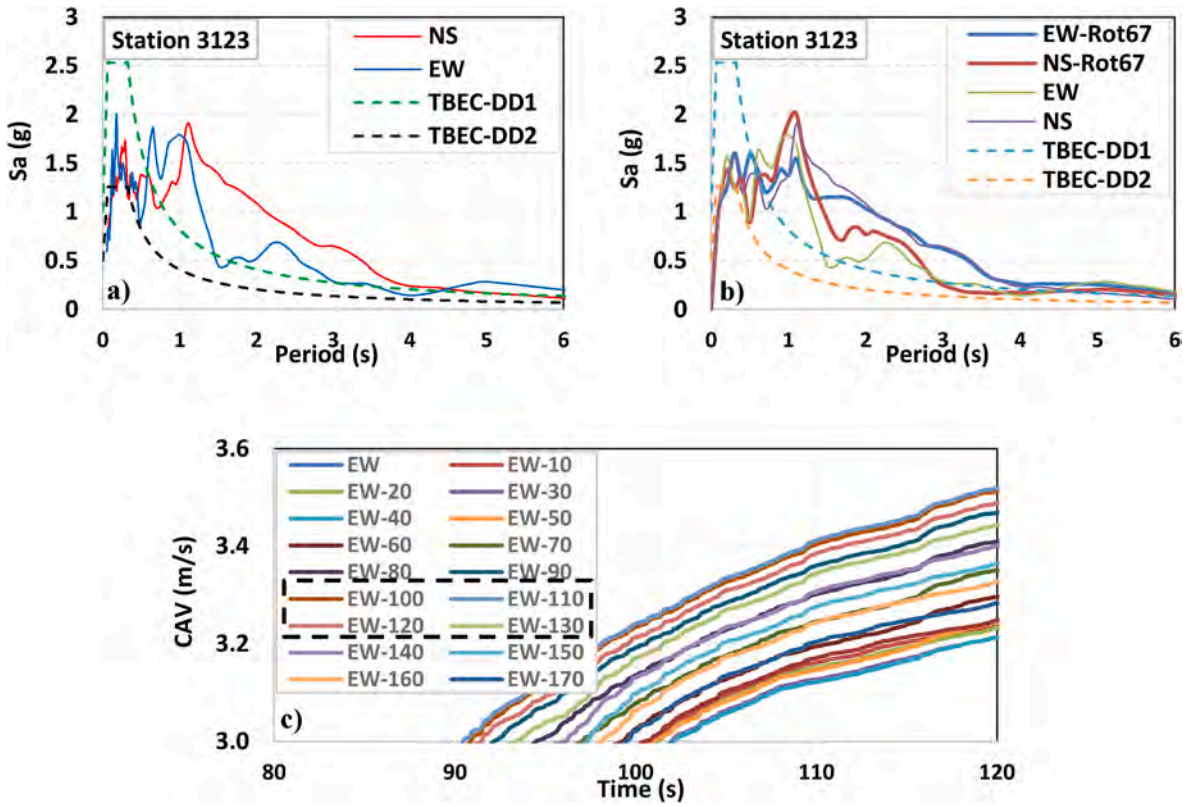

Fig. 15. a) Comparison of acceleration spectra, b) the rotated acceleration spectra and, c) CAV values for station 3123.

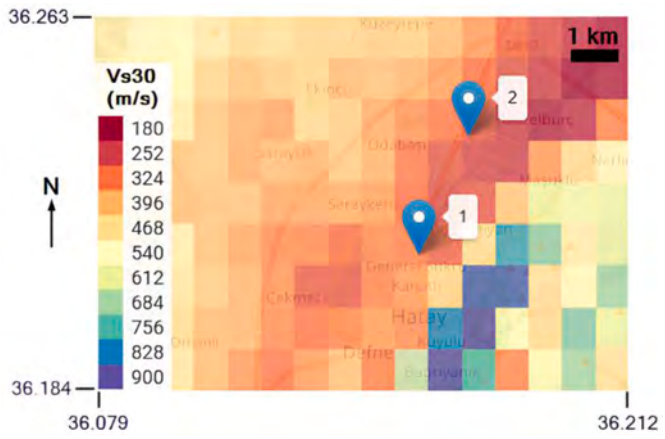

Fig. 16. Comparison of $V_{s,30}$ values for stations 3123 (point-1) and 3124 (point-2) [79].

component are higher than the DD1 design values in the 0.6–0.9s and 2–4s ranges, whereas the NS component shows higher spectral accelerations in the 2.1–4s range (Fig. 17a). According to Table 2, Hu et al. [22] and Baltzopoulos et al. [1] identified velocity pulses with periods of approximately 3.4s at azimuth angles of 117° and 135°, respectively. Chang et al. [19] identified a pulse orientation at 90°, suggesting the presence of forward directivity effects. The pulse data and acceleration spectra for the components of this station indicate velocity pulses at azimuth angles between 90° and 135°, while the pulse-like characteristics diminish in the fault-parallel orientation at 67°. Thus, it is not possible to clearly identify a supershear effect, which is expected to be prominent in the fault-parallel direction, based on this perspective. Fig. 17a illustrates the acceleration spectra obtained by rotating the original recording by 67° to align with the fault-parallel orientation, while Fig. 17b presents the spectra for the original recording rotated by 135° to align the original EW component with the pulse orientation. As shown, no pulse trace or corresponding acceleration amplification is observed in the fault-parallel orientation, whereas high spectral accelerations are evident in the 2–4s period range in the fault-normal orientation. These results suggest the presence of forward directivity in the data from station 3125 but do not provide evidence for supershear

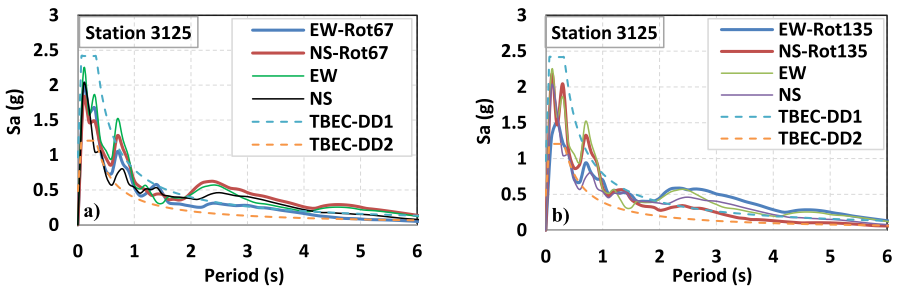

Fig. 17. Acceleration spectra obtained by rotating the original 3125 components by a) 67° and b) 135°.

effects. Additionally, the spectral accelerations at this station are not as high as those recorded at stations 3129, 3123, and 3124, indicating that if a supershear effect exists in this region, it is less pronounced than in the other locations. Moreover, the absence of geological features conducive to basin effects in station 3125 area contributes to the relatively lower recorded accelerations. This lack of basin amplification is a significant factor in the observed differences.

The orientation-dependent evaluation of seismic energy was conducted using CAV (Cumulative Absolute Velocity) values. For this purpose, CAV values were calculated for every 10° rotation angle from 0° to 180°. The energy released during an earthquake is significantly influenced by its effective duration [63]. To evaluate this aspect, a Husid plot was utilized to identify the significant duration of the recording, which was determined to span the interval between 72 and 89 s (Fig. 18a). Finally, the orientation corresponding to the maximum CAV value was determined and plotted for each second within the significant duration interval (Fig. 18b). The results indicate that during the initial pulse seconds of the earthquake, high energy levels aligned with the pulse orientation (130°). However, in the subsequent seconds, the CAV values deviated from the pulse orientation and reached their maximum at orientations of 30°, 40°, and 50°. The absence of a pulse in the fault-parallel orientation and the distribution of CAV values suggest a gradual shift of energy toward the fault-parallel direction. Given these findings, it is challenging to confirm the presence of a potential supershear effect based on the recordings from station 3125. Evidence supporting forward directivity effects is apparent; however, conclusive inferences regarding supershear phenomena cannot be substantiated. To address this limitation, further investigations are necessary to deepen the understanding of this issue, as alternative interpretations may arise from advanced research. High-resolution seismic simulations, employing comprehensive fault modeling and incorporating a broader range of parameters, have the potential to yield novel insights into the seismic characteristics recorded at station 3125.

3.2.5. Station 3126

The spectral acceleration values for the EW and NS components of the 3126 station recordings exceed the TBEC 2018 [31] DD1 design accelerations, even for periods up to the 0.4-s threshold. In this region, particularly for the NS component, the accelerations are approximately twice those of the EW component. NS component accelerations reaching up to 4–5g suggest the potential influence of supershear effects. For periods longer than 0.4 s, the EW spectral accelerations are consistent with the DD1 spectrum, whereas in the NS component, DD1 acceleration exceedances are observed in the 1.7–4 s range (Fig. 19a).

The identification of velocity pulses in the horizontal components of the 3126 station recordings has yielded differing results among researchers (Table 2). The pulse identified by Hu et al. [22] at an azimuth angle of 158° does not correspond to a distinct acceleration amplification region in the NS component acceleration spectrum when the original record is rotated by 67° (Fig. 19a). Conversely, the pulse effect identified by Baltzopoulos et al. [1] at an azimuth angle of 112° is observed as high accelerations in the 2–4s period range in the EW component of the spectrum for the rotated dataset (Fig. 19b). However, in Fig. 19a, the acceleration spectrum of the EW component, which represents the fault-parallel direction, exhibits a more prominent peak in the 1.7–3s period range. This observation could indicate the presence of a pulse-like effect in the fault-parallel direction, potentially attributed to supershear phenomena. This hypothesis, requiring further validation through detailed investigations, is also supported by the CAV values. As shown in Fig. 20a and b, the orientations yielding the highest CAV values fall within the 80°–100° range. Moreover, during the significant time interval of 70–90 s—associated with significant duration and velocity pulses—the CAV values in these orientations are more pronounced. Thus, seismic energy concentrated in and active along the fault-parallel orientation can be inferred. In Fig. 20c, the orientation maximizing CAV values over time begins with the velocity pulse orientation and subsequently aligns with the 80° direction. In conclusion, the azimuth angle of the pulse definition, the orientations associated with maximum CAV values in the dataset, and the extremely high acceleration values observed in the spectra suggest that a possible supershear effect may have influenced station 3126 region. However, this assumption requires confirmation through more detailed studies.

3.2.6. Stations 3131 and 3132

The comparisons of TBEC 2018 design spectra with the acceleration spectra recorded at 3131 and 3132 stations are presented in Fig. 21a and b, respectively. Among the Antakya region stations, the spectral accelerations at 3131 exhibit the lowest values. At this station, while the DD2 design accelerations are exceeded for periods longer than 0.6 s, the DD1 design accelerations are not surpassed at any period range. In contrast, the spectral accelerations at 3132 are slightly higher than those at 3131. For station 3132, the spectral accelerations exceed the DD2 design values for periods longer than 0.4 s in the EW component and longer than 0.6 s in the NS component. Additionally, while the EW component slightly surpasses the DD1 design values in a narrow period range (0.7–1.2 s), the NS component shows significant exceedances in the 0.9–1.5 s period range. In terms of velocity records, the 3131 station exhibits a pulse-like characterization, but the identified pulse periods are significantly longer. These extended pulse periods are significantly different from the natural periods of buildings in the region, suggesting that their impact on structural damage was relatively limited. For the 3132 station, velocity records have not been characterized as pulse-like by researchers (Table 2). The lack of clear velocity pulse signatures and the relatively low recorded acceleration amplitudes compared to other stations suggest that supershear effects are not observed at these stations. Abdelmeguid et al. [24] observed that although the presence of supershear effects at station 3132 cannot be entirely ruled out, they remain inconclusive. Additionally, they identified the shear wave velocity at station 3131 as characteristic of the sub-shear velocity regime.

The NS component acceleration spectrum at approximately 1-s periods presents a peak acceleration region that could be interpreted as a potential supershear indicator at station 3132. These elevated accelerations in this range may result from a possible pulse effect. Given that the NS component is oriented near the fault-parallel direction, any pulse traces in this orientation could potentially be linked to supershear phenomena. The effective duration values for station 3132 were

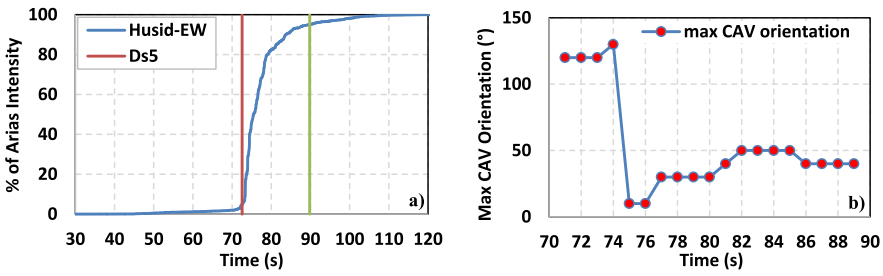

Fig. 18. a) Husid diagram and, b) maximum CAV orientations for station 3125.

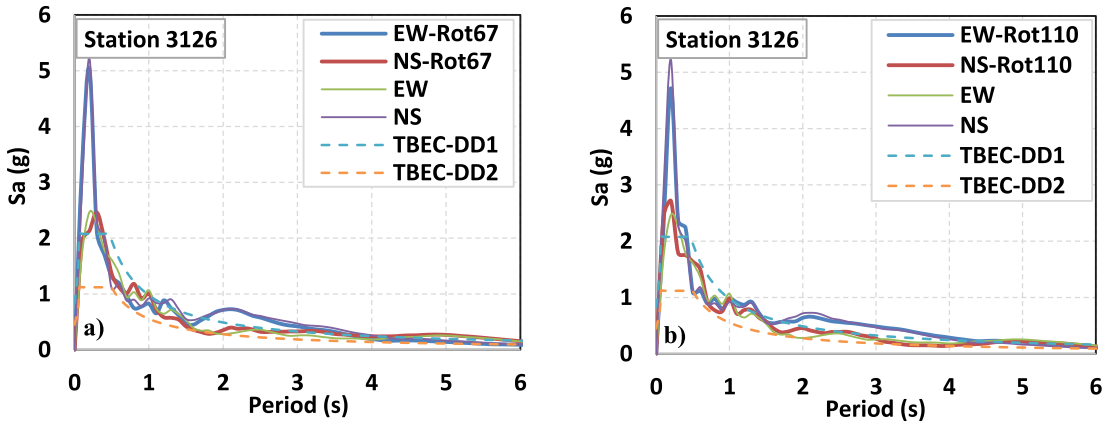

Fig. 19. Comparison of acceleration spectra by rotating the record as; a) 67° and b) 110°.

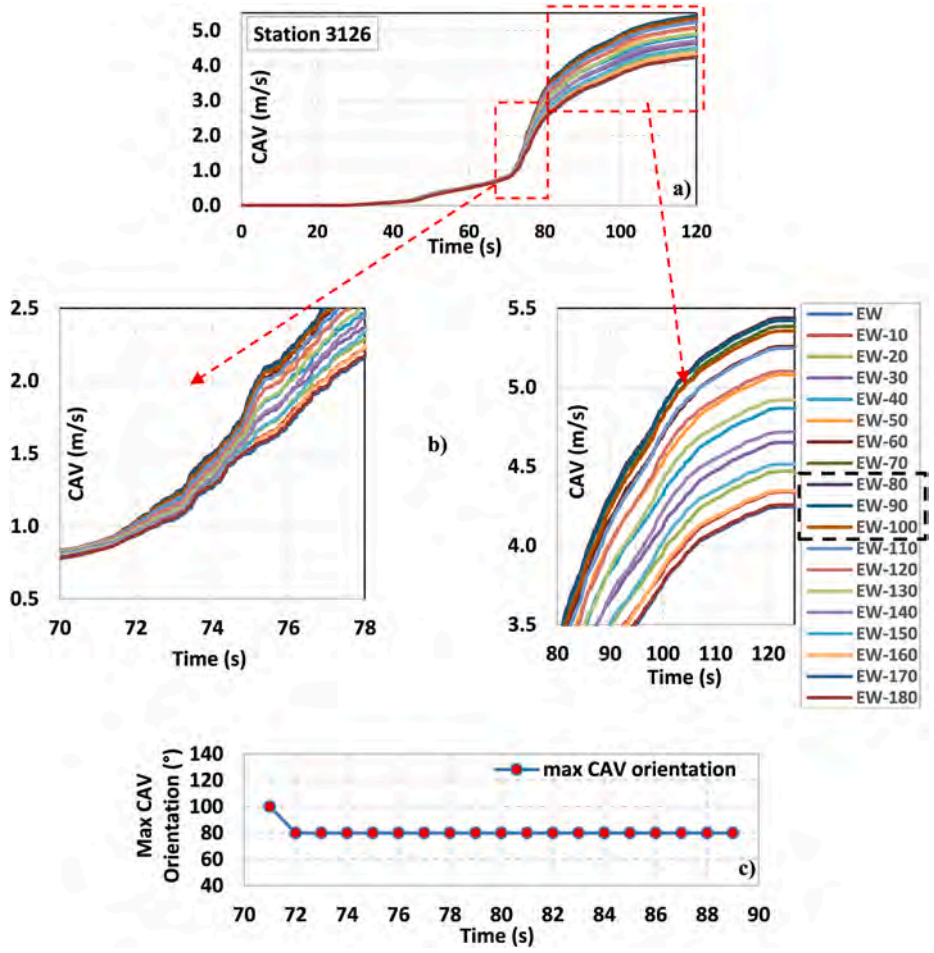

Fig. 20. a) Highest CAV values in different time intervals, b) CAV graphs for specific time intervals, c) orientations maximizing the CAV values for station 3126.

calculated as 17.61 s for the original EW component (Fig. 22a) and 13.45 s for the NS component (Fig. 22b). This suggests that energy concentration near the fault-parallel direction may be attributed to a pulse-like effect in the NS component. To further analyze this, the record was rotated by 67° to align the original EW component with the fault-parallel direction (FP), and the acceleration spectra of the components were plotted alongside the original spectra (Fig. 22c). The peak accelerations observed in the 1-s period range of the FP component were found to be lower than those of the original NS spectrum. Additionally, the significant duration for the FP orientation increased to 16.58 s. This observation indicates that a pulse-like effect might be present in orientations between 90 and 100°.

To identify the orientations associated with higher CAV values, the record set was rotated in 10-degree increments, and CAV graphs were plotted for each direction over the earthquake duration, along with the orientations yielding the highest time-dependent CAV values (Fig. 23a and b). The time interval considered in Fig. 23b corresponds to the significant duration range of 71–90 s across all orientations. The highest

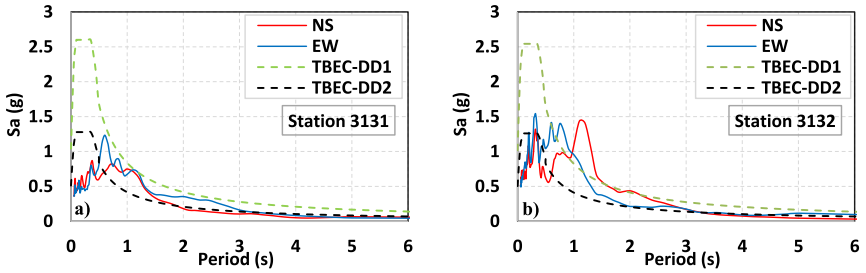

Fig. 21. Comparisons of seismic code spectra with the acceleration spectra recorded at a) 3131, b) 3132.

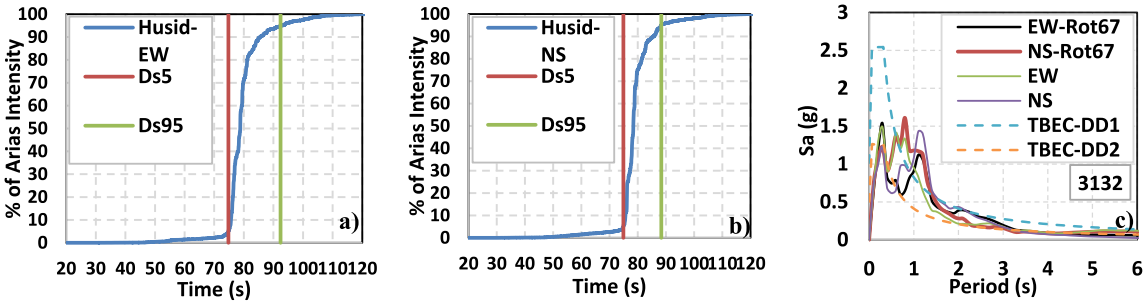

Fig. 22. The effective durations for station 3132; a) EW component, b) NS component, and c) acceleration spectra of the components.

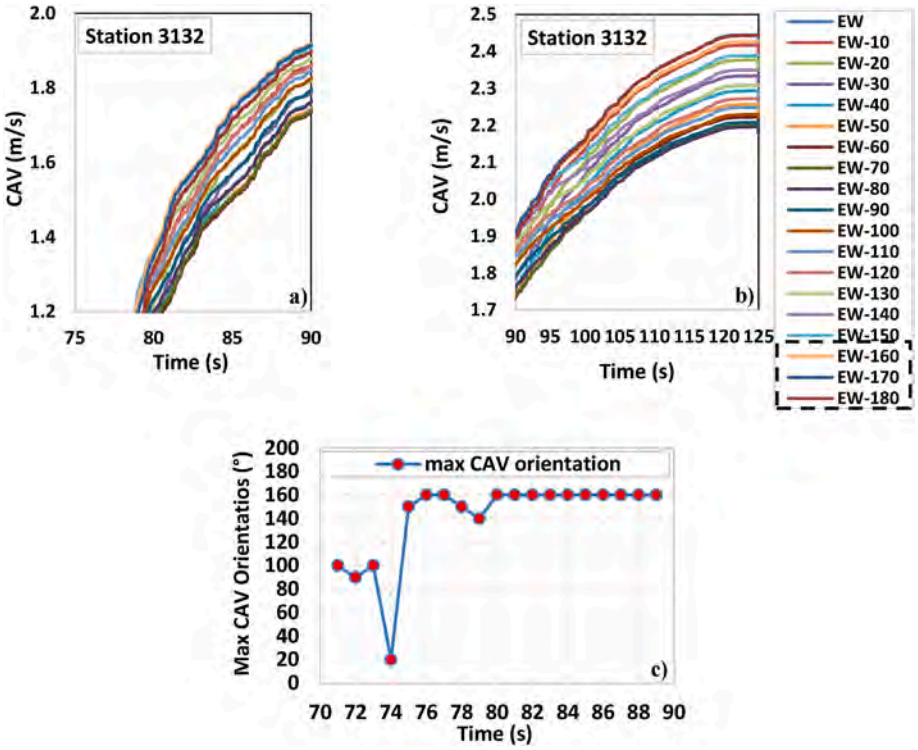

Fig. 23. a) CAV values for Station 3132, b) a closer view of the maximum CAV values, c) max CAV values corresponding to the 160° orientation.

CAV values for the entire earthquake duration were observed in the 160–170-degree orientations, which align with the fault-normal direction (Fig. 23a and b). During the initial seconds of the significant duration, a pulse-like seismic wave was generated in the 90–100-degree orientations, consistent with the rise in 1-s spectral accelerations in the original NS component. However, this effect did not exhibit a dominant pulse character comparable to those observed at other stations. Subsequently, due to wave propagation, energy was released in the fault-normal direction, with the highest CAV values corresponding to the 160-degree orientation (Fig. 23c). Nevertheless, the energy released in the fault-normal direction does not exhibit a pulse-like nature, which explains the absence of high and abrupt increases in acceleration at this station. In conclusion, effects such as supershear and directivity did not leave significant traces at this location.

It is evident that the recorded ground motion accelerations at stations 3131 and 3132 exhibit distinct characteristics compared to other

stations. Since these stations are near stations 3123 and 3124, it is challenging to attribute the recorded ground accelerations to seismic parameters such as the fault system or distance from the fault. Therefore, the primary factor contributing to these differences is likely to be geological and topographical characteristics. The 3131 and 3132 regions have ground properties that significantly differ from those of other stations. Located at the foot of Mount Habib-i Neccar, the ground in these areas is quite firm, and the absence of site effects causing acceleration amplification is natural (Fig. 24a). The recording of the lowest ground accelerations at station 3131 and the lack of close fault effects support this view, as station 3131 is situated in a relatively high mountainous area compared to other stations. Station 3132, located at a lower elevation on the mountain's foothills, may exhibit potential traces of nearby fault effects. Fig. 24b presents a map of the estimated $V_{s,30}$ values for these stations. Markers 1 and 2 on the map represent stations 3131 and 3132, respectively. The $V_{s,30}$ values are significantly higher in the mountainous region, but they decrease considerably as one moves toward the valley center. The hard ground in the rear area of the stations and the soft ground in the valley may significantly alter wave propagation, causing fractures and reflections. Therefore, the geological and topographical conditions created by the mountainous terrain at the rear of these stations likely play a role in the recorded ground accelerations, as seismic energy propagates along the fault rupture direction.

4. Vertical ground motion in Antakya

One of the most notable features of the February 6 Pazarcık earthquake was the exceptionally high vertical acceleration values recorded, as reported by numerous researchers [7,32,70]. Traditionally, vertical earthquake acceleration is estimated to be approximately two-thirds of the horizontal acceleration, a principle established by Newmark et al. [71] and widely adopted in design codes. However, past earthquakes such as Loma Prieta (1989), Kobe (1995), and Kocaeli (1999) have shown cases where vertical accelerations equaled or exceeded horizontal accelerations. Elnashai and Papazoglou [72] emphasized that this two-thirds threshold is not universally applicable, particularly in near-fault earthquakes. Modern guidelines, including IBC-2000 [73] and ASCE/SEI 7–16 [74], allow for adjustments to this coefficient to account for variability in seismic behavior. In the Turkish Building Earthquake Code (TBEC-2018) [31], vertical earthquake effects are addressed using two methods. The first involves defining a vertical acceleration design spectrum derived from the horizontal spectrum parameters. Key parameters, such as the short-period spectral acceleration (S_{DS}), corner periods (T_{AD} and T_{BD}), and the transition period to the constant displacement region (T_{LD}), are calculated based on the horizontal spectrum. The second method simplifies vertical effects by multiplying dead loads by two-thirds of the S_{DS} value. TBEC-2018 mandates the first method for specific structural elements, such as beams with spans over 20 m, cantilevers exceeding 5 m, and buildings with inclined columns or columns resting on beams. For other structures, the second method is used, with the maximum vertical acceleration set as two-thirds of the horizontal spectrum's plateau value. These provisions ensure that vertical accelerations, particularly in near-fault zones where amplification is significant, are adequately considered in structural designs.

The vertical acceleration spectra recorded at stations in the Antakya region were compared with the TBEC 2018 vertical design spectra (Fig. 25). The DD1 vertical design spectrum values were exceeded at all stations except station 3131. Additionally, V/H ratios significantly surpassed the 2/3 threshold in the short-period range across all stations.

Duan et al. [2] identified the trampoline effect as a key factor contributing to extremely high vertical accelerations. This effect occurs when positive vertical accelerations exceed negative ones, generating significant dilatational stresses due to strong downward accelerations. These stresses can lead to tensile cracking and void formation in near-surface soils, effectively reaching the soil's tensile strength and causing a loss of cohesion. The phenomenon is analogous to the upward thrust experienced by a mass bouncing on a trampoline, where the upward force surpasses gravitational pull [30]. Analysis of vertical components recorded at Antakya stations supports the trampoline hypothesis. As shown in Fig. 26, the positive vertical accelerations (blue) exceed the absolute values of the negative accelerations (red) at all stations except for Station 3131.

Fig. 27a compares the CAV values of discrete positive and negative accelerations, showing that positive acceleration CAV values are higher at all stations except 3131. This difference is particularly pronounced at stations 3123 and 3129, with the highest CAV values recorded at station 3126. A key indicator of the trampoline effect is the ratio of maximum positive to maximum negative vertical acceleration, which is expected to exceed 1. As shown in Fig. 27b, this ratio surpasses 1 at all stations except 3131 and 3132. Notably, while station 3132 recorded a peak acceleration ratio of 0.9, the vertical acceleration time histories indicate that upward amplitudes are generally higher.

The presence of vertical acceleration pulses is a critical factor in identifying the trampoline effect [30,75]. While velocity pulses associated with phenomena such as directivity, fling, and supershear have been identified in the horizontal components of records, vertical acceleration analyses show no clear evidence of a combination with supershear or directivity effects. Station 3125 does not exhibit the characteristic features of supershear traces observed at other stations but shows similar vertical acceleration results to stations other than 3131 and 3132. Station 3124 displays supershear signatures but shares a similar CAV profile with station 3132, where the presence of supershear traces remains uncertain. These results are influenced by numerous parameters. The ground does not become entirely cohesionless, as factors such as material friction, mechanism complexity, and nonlinear behavior significantly affect the trampoline effect. Additionally, seismic wave characteristics, topographic conditions, and soil type play crucial roles. For instance, soft soils are more likely to reach their tensile strength and lose cohesion compared to stiff soils. Amplification of upward vertical accelerations is more pronounced in highly damped soft soils due to increased ground amplification. However, vertical acceleration amplitudes recorded at station 3124, located in a relatively softer soil region, are lower than those observed at other stations except 3131 and 3132. The regions of stations 3131 and 3132, situated on the slopes of Habib-i Neccar Mountain, feature exceptionally stiff soil conditions, while the other stations are located within a valley underlain by softer soils. These topographic and soil conditions likely explain the differences in results between stations 3131 and 3132 and the others. To

Fig. 24. a) Stiff soil at the foothills [76], b) the map of the estimated $V_{s,30}$ values for 3131 (Point-1) and 3132 (Point-2) [79].

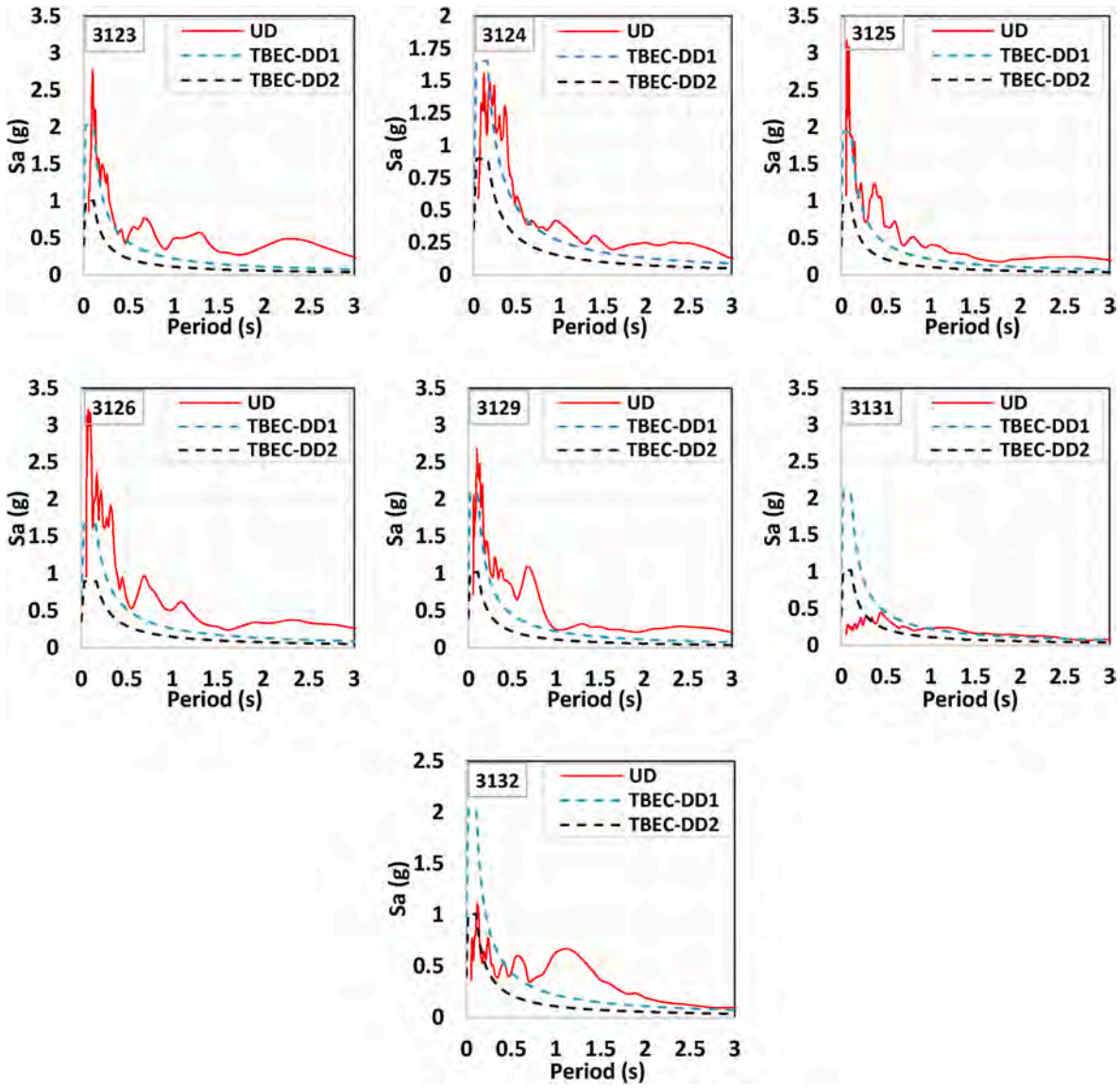

Fig. 25. Comparison of the vertical acceleration spectra proposed by the TBEC 2018 and Antakya stations.

substantiate these observations, further studies incorporating complex fault systems, multilayered soil structures, and nonlinear behaviors are necessary.

5. Building damages based on station locations

The destruction and damage caused by the Pazarcık earthquake in the Antakya district were analyzed at the neighborhood scale, with the results presented in Table 3. Neighborhoods are categorized based on their proximity to the nearest seismic recording stations. In addition to locational characteristics, three primary parameters—building age, story count, and soil properties—were included, as damage assessment cannot rely solely on locational data. Neighborhood names, building counts, and damage states were obtained from the dataset available on the ministry's website [36]. Building age was classified into three categories: Young (0–15 years), Moderate (15–30 years), and Aged (over 30 years), represented by their initials in the table. Story count was categorized as Low (1–4 stories), Medium (5–8 stories), and High (more than 8 stories), excluding rigid basement levels. These classification thresholds were selected to best reflect the regional building stock. Open sources [76–78] were used to identify these data, and streets were manually reviewed while buildings were digitally examined to ensure representativeness. In cases where no clear trend in building age or story count was observed, multiple types were listed, with the most prominent type highlighted in bold. Soil properties were evaluated using estimated $V_{s,30}$ shear wave velocities obtained from the Global $V_{s,30}$ Map [79]. For neighborhoods with multiple $V_{s,30}$ values, the data are presented as a range. The building stock in the area primarily consists of multi-story, multi-span reinforced concrete structures. As indicated in the table, damage severity is represented by shades, with darker shades corresponding to higher damage percentages. This methodology integrates multiple parameters—locational data, building characteristics, and soil properties—to provide a comprehensive assessment of building stock and damage distribution, capturing the complexity of the earthquake's impact.

In the vicinity of Station 3123, the calculated ratios for E + F and D damage levels are approximately 36 %, with heavily damaged and destroyed buildings accounting for 71 %—the highest value in Table 3. The neighborhoods with the most severe destruction (Akevler, Cebrail, Cumhuriyet, Emek, General Şükrü Kanatlı) predominantly consist of low-to medium-rise, moderate-aged buildings. Even for 2–3 story buildings, predominant periods are at least 0.4–0.5 s due to outdated designs lacking reinforced concrete shear walls. Additionally, older buildings often have insufficient column dimensions and inadequately

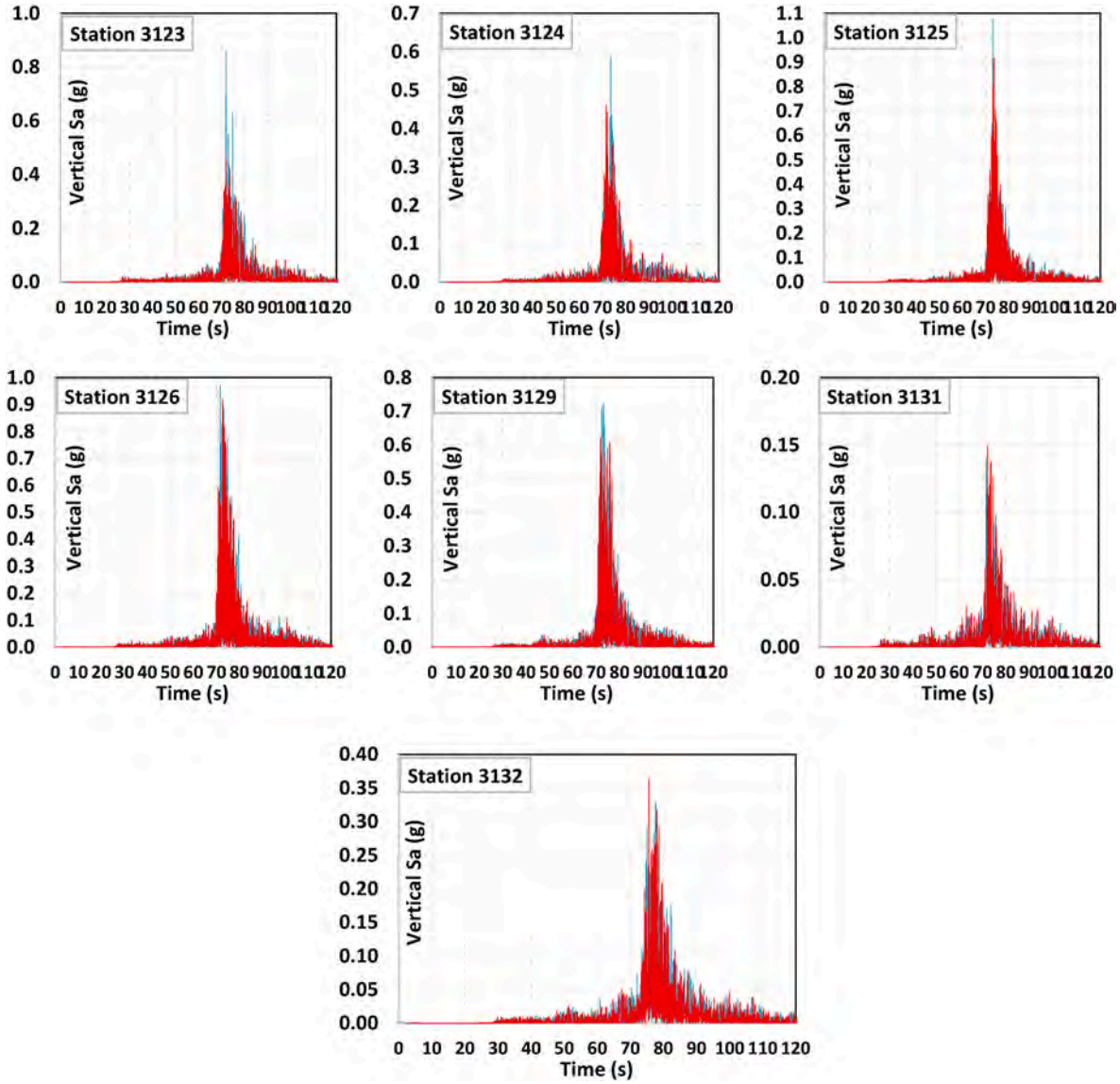

Fig. 26. The positive and the absolute negative vertical accelerations for each station.

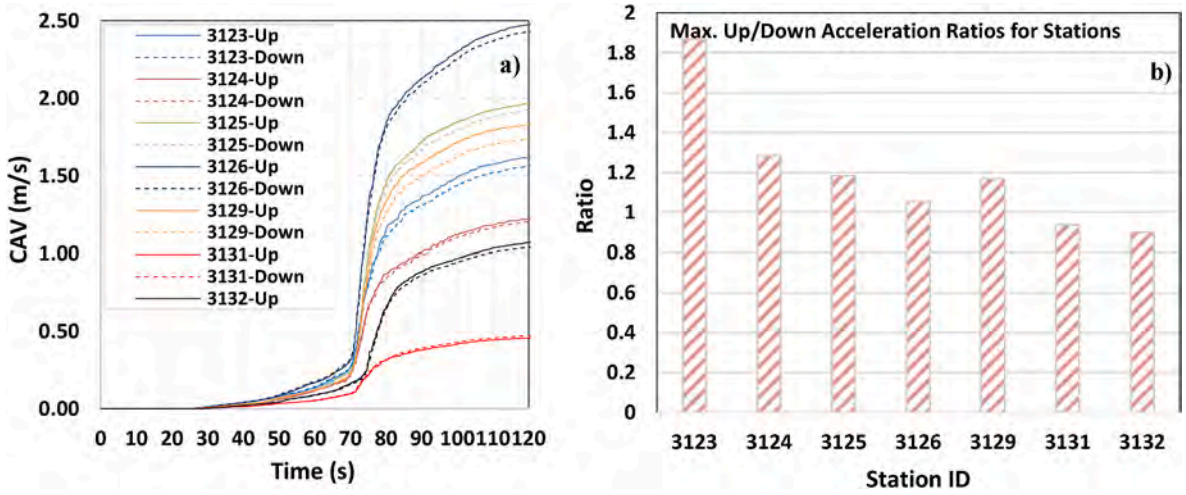

Fig. 27. a) Comparison of the CAV values of discrete positive and negative accelerations, b) maximum upward/downward acceleration ratios for each station.

Table 3
The relationships between the station records, building damage conditions, and soil classification of neighborhoods in the Antakya district.

Station ID	Neighborhood	Number of Buildings	Building Age	Number of Story	Vs30 (m/s)	Immediate Demolition and Collapsed (E+F)[1]	Severely Damaged (D)[1]	E+F (Based on Station ID)[2]	D (Based on Station ID)[2]	E+F+D (Based on Station ID)[2]
3123	Akevler	805	M	M	350-370	39.8%	32.7%	36%	36%	71%
	Cebrail	463	M, **A**	M	340-375	74.3%	20.7%			
	Cumhuriyet	537	**M**, A	M	340-350	56.1%	34.1%			
	Emek	1252	M, **A**	L	340	45.9%	46.2%			
	Esenlik	824	**M**, A	L, **M**	290-345	23.3%	40.7%			
	G. Ş. Kanatlı	522	**M**, A	M	340-375	65.7%	20.9%			
	Haraparası	813	A	L	320-460	25.8%	42.3%			
	Küçükdalyan	1062.5[3]	M, **A**	L	280-500	18.8%	27.3%			
	Ürgen Paşa	1040	M	M	320-370	32.2%	32.6%			
	Güllü Bahçe	185	A	L	350	34.1%	41.6%			
	Zenginler	353	A	L	350-800	35.4%	56.4%			
	Meydan	577	A	L	460	19.6%	52.2%			
	Ulucamii	292	A	L	350-800	50.7%	42.1%			
	Yeni Camii	781	A	L	815	14.0%	21.9%			
3124	Güzelburç	3779	A	L	220-300	25.5%	14.4%	23%	20%	43%
	Kuzeytepe	953[3]	A	L	380-460	15.3%	17.1%			
	Küçükdalyan	1062.5[3]	A	L	280-500	18.8%	27.3%			
	Maşuklu	1434	A	L	220-600	15.3%	17.4%			
	Odabaşı	2110	Y, **M, A**	L, M, H	290-370	30.4%	30.3%			
3125	Ekinci	1915	M, **A**	L	385-460	3.0%	25.2%	5%	32%	37%
	Günyazı	625	M, **A**	L	388	1.1%	29.1%			
	Saraycık	135	A	L	380-420	11.9%	43.7%			
	Saraykent	776.5[3]	Y, **M**	M	375-440	11.3%	47.5%			
3126	Akasya	2047	Y, **M, A**	L, **M**	320-390	7.9%	52.1%	16%	51%	67%
	Aksaray	1047	M, A	L, M	290-330	12.0%	55.8%			
	Altınçay	1168	M, **A**	L, M	290-350	34.1%	44.9%			
	Esentepe	703	M, A	L, M	290	20.2%	51.4%			
	Saraykent	776.5[3]	**M**, A	L, M	375-440	11.3%	47.5%			
3129	Akdeniz	256	M	M	340	1.6%	40.6%	24%	41%	65%
	Armutlu	643	M, **A**	L, **M**	340-370	34.1%	49.3%			
	Aşağıokçular	289.5[3]	M	M	310-480	5.5%	15.9%			
	Elektrik	339	**A**	**L**, M	370	65.8%	29.5%			
	Subaşı	1055	Y, **M, A**	L, M	320-420	10.4%	35.5%			
	Turunçlu	916	M, A	**L**, M	340-440	9.3%	53.5%			
	Gazi	784	M, **A**	M	340-375	45.8%	37.5%			
3131	Dursunlu	1200	M, **A**	**L**, M	600-700	6.4%	20.1%	12%	24%	36%
	Sümerler	712	M, **A**	**L**, M	340-600	11.1%	23.2%			
	Bağrıyanık	917	A	L	900	1.3%	4.0%			
	Fevzi Çakmak	274	A	L	800	26.6%	33.9%			
	Gazi Paşa	210	A	L	815	11.9%	53.3%			
	Havuzlar	318	A	L	900	1.3%	4.4%			
	Kantara	279	A	L	815	40.5%	43.0%			
	Kışla Saray	327	**M**, A	L, **M**	350-650	20.5%	44.3%			
	Kuyulu	344	A	L	815	27.9%	34.6%			
	Şehitler	221	A	L	815	34.8%	32.6%			
	Şirince	384	A	L	815	5.2%	29.7%			
3132	Aydınlıkevler	465	A	L	870-900	1.3%	3.9%	13%	26%	39%
	Barbaros	50	A	L	815	42.0%	54.0%			
	Biniciler	192	A	L	815	32.8%	59.4%			
	Dutdibi	224	A	L	815	30.8%	29.5%			
	Habib-i Neccar	115	A	L	815	20.0%	29.6%			
	Hacı Ömer Alpagot	1003	A	L	870	2.8%	12.5%			
	İplik Pazarı	138	A	L	815	27.5%	68.1%			
	Karaali Bölüğü	434	A	L	815-900	1.4%	14.5%			
	Kardeşler	433	A	L	815-900	11.3%	19.9%			
	Kocaabdi	123	A	L	815	46.3%	30.9%			
	Orhanlı	340	A	L	460-800	23.8%	29.7%			
	Sofular	354	A	L	800-900	13.8%	43.2%			
	Şeyhali	198	A	L	815	24.2%	64.6%			

[1] Neighborhood percentages were obtained from https://hasartespit.csb.gov.tr/ based on the corresponding damage status.
[2] Percentages for the station were calculated using the damage data of the corresponding neighborhoods.
[3] Half of the total number of buildings was excluded due to the station's distance or the neighborhood's unsuitable layout.

designed beam systems, resulting in low stiffness and longer predominant periods. For 5–6 story buildings, regardless of age, predominant periods exceed 0.6 s. Moderate-aged buildings frequently exhibit deficiencies in material strength (concrete and reinforcement grades), quantity (ratios of longitudinal and transverse reinforcement), and detailing (anchorage, lap splices, and hook designs). These deficiencies hinder confined concrete behavior and ductile performance, leading to rapid elongation of periods after plastic deformations and increased structural damage. Spectral accelerations from the 3123 ground motion records are significantly amplified beyond 0.6 s, subjecting buildings to very high ground accelerations. Soil properties further exacerbate the damage. The soil near Station 3123 is weak, with $V_{s,30}$ values ranging between 280 and 370 m/s, indicating soft soil with a long predominant period. This amplifies seismic effects at longer periods, intensifying the destructive impact on long-period structures. In contrast, neighborhoods with lower destruction rates, such as Yeni Camii, Küçükdalyan, and Meydan, feature predominantly older buildings but benefit from stiffer soils. In areas with varying $V_{s,30}$ values, the correlation between collapse rates and soil stiffness is critical. For example, in Ulucamii and Zenginler neighborhoods, $V_{s,30}$ values reach up to 800 m/s in the eastern parts near the foothills, where stiffer soils are located. However, the collapsed sections are situated in the western parts near the riverbed, where softer soils result in higher destruction rates. In summary, the combination of supershear, directivity, and basin effects likely contributed to the elevated ground accelerations and severe destruction observed near Station 3123.

The situation around Station 3124 is similar to that of Station 3123. Except for Odabaşı neighborhood, buildings are typically low-rise and older, while Güzelburç, located on a riverbed with softer soil, exhibits the highest destruction rates due to basin effects. In contrast, soils in other areas become stiffer toward mountainous terrains, correlating with lower damage ratios. Odabaşı neighborhood shows notable near-fault effects. Many medium-to high-rise buildings near the Asi River, constructed after 2010 under the 2007 earthquake code with reinforced concrete shear walls, collapsed or were severely damaged during the Pazarcık earthquake. Historical Google Earth images indicate significant construction activity in this area between 2010 and 2022, with many new buildings designed according to the 2007 earthquake code and incorporating reinforced concrete shear walls (Fig. 28). Low-rise, older buildings are typically located outside this region. The collapse of seven- to eight-story or taller buildings is attributed to high spectral accelerations beyond 2 s, amplified by pulse-like near-fault ground motions and soil conditions. The strong near-fault effects at Station 3124, including supershear and directivity traces, significantly contributed to the destruction.

The area surrounding station 3126 is characterized by medium-aged buildings, predominantly low to moderately tall structures. There is no clear trend in building height or age in the region; however, Akasya neighborhood stands out as having the youngest building stock, while Altınçay is the oldest, a fact reflected in the percentages of collapsed buildings. The very high spectral accelerations observed in the 3126 station records are mostly associated with short periods. Consequently, the seismic response of structures in this area showed low sensitivity to these high accelerations. This is because the buildings in the 3126 region are low and moderately tall, and given the soil period, they are more susceptible to vibrations in longer periods. Nevertheless, the proportion of heavily damaged buildings in the 3126 region is notably high at 51 %. This outcome can be attributed to the relatively newer building stock's capacity to exhibit ductile behavior, which allowed many structures to remain standing despite sustaining severe damage. Broadly speaking, it can be concluded that older buildings were destroyed while newer structures absorbed seismic impacts through significant damage. Additionally, considering the increase in spectral accelerations beyond 2 s, it is unsurprising that even newer buildings experienced more damage than anticipated.

The area surrounding station 3129 represents the second-highest location in terms of destruction rates. The very high short-period accelerations observed in the acceleration spectra of strong ground motion records, along with the high accelerations in the 1–2 s period range of the NS component, significantly contributed to the increase in damage and destruction. Neighborhoods with the highest destruction rates were found to be those situated on softer soils, where a substantial number of older buildings are present. Conversely, neighborhoods such as Akdeniz and Aşağıokçular, which consist of relatively newer buildings, or Turunçlu, which features low-rise buildings on stiffer ground, exhibited reduced destruction rates.

The area surrounding station 3125 exhibits the lowest destruction rate. Analysis of ground motion records from this region shows no evidence of supershear effects. The building stock in the 3125 region falls predominantly within the moderate and aged categories, but most of these structures are low-rise. Additionally, the area's ground conditions lack characteristics that would amplify seismic waves. Similarly, the destruction rates in the areas surrounding stations 3131 and 3132 are significantly lower compared to other stations. A notable characteristic of the neighborhoods near these stations is the prevalence of very old buildings. These structures are typically 2–3 stories tall and exhibit cross-sectional and reinforcement properties far from modern standards. Despite their lack of engineering design and evident weaknesses in strength, ductility, and stiffness, the survival of these buildings in such a major earthquake is noteworthy. The primary factor contributing to the survival of these buildings is the soil properties of the region. The areas around stations 3131 and 3132 are situated on the foothills of mountains, where the soil is exceptionally stiff. Due to the soil composition and mountainous terrain, phenomena observed in other regions such as

Fig. 28. Building stock in the Odabaşı region over different years [76].

high accelerations, velocity pulses from near-fault effects, and supershear-directivity-basin interactions were not significant in these locations. The critical role of soil and topographical properties in this outcome is illustrated in Fig. 29a. As shown, moving towards the river basin where the soil becomes softer, the level of destruction and damage significantly increases. In the acceleration spectra of ground motion records, high values are observed for periods exceeding 0.6 s. However, the rigid soil near the foothills ensures that the dominant soil frequency remains at relatively high levels. This results in the seismic effects being dampened by the ground itself, as the building frequencies fall outside the dominant soil frequency range. In contrast, in the river basin region, where the soil is softer and the dominant soil frequency is lower, the building frequencies align more closely with the soil frequencies. This alignment allows ground accelerations to be transmitted to the buildings, leading to greater levels of destruction.

The percentages of the damage conditions "Immediate Demolition" + "Collapsed" (E + F), "Severely Damaged" (D), and the total of these damage conditions (E + F + D) presented in Table 3 are summarized in graphical form by station in Fig. 29b. As seen in the graph, the regions with the highest destruction are 3123, 3124, and 3129 stations. The highest percentages of severely damaged buildings are found in the 3126 and 3129 stations, where the characteristics of the building stock and local soil conditions, as summarized in Table 3, play a significant role in this result. When buildings are younger, the demolition rates decrease, but the percentage of severely damaged buildings increases. When considering the E + F + D damage conditions together, the highest percentages are observed at 3123, 3124, 3126, and 3129. These results indicate that damage and destruction have increased in stations exhibiting signatures of supershear, directivity, and basin effects.

The magnitude of vertical acceleration values during the earthquake played a significant role in the damage observed in buildings in the Antakya region. Vertical earthquake effects exacerbated damage in older buildings due to poor concrete and reinforcement quality, insufficient lap splices and anchorage lengths, and inadequate strength and stiffness of structural systems. Furthermore, even in relatively younger buildings, severe damage was observed at the upper ends of columns or beam-column joints. Such damage occurred due to factors such as the shear capacity of the joint being exceeded, a reduction in column flexural moment capacities under tensile forces, and the loss of ductile behavior in columns under high compressive forces. Vertical earthquake effects were found to significantly contribute to increased damage levels or even building collapse under these conditions. Fig. 30a illustrates an example of crushing, tension, bending, and punching shear damage caused by vertical effects in a building with poor concrete quality and insufficient/inappropriate reinforcement placement. In such buildings, the reduction in column flexural moment capacities under tensile forces in vertical load-bearing elements often leads to excessive plastic deformation and stability losses in many columns. This phenomenon is frequently observed, particularly in high-rise buildings, where vertical earthquake accelerations facilitate the complete overturning of the structure. For instance, as shown in Fig. 30b, in a 10-story building, damage to load-bearing elements resulted in a reduction in structural stiffness, leading to increased lateral displacements. Vertical earthquake effects further amplified second-order effects in buildings with increased lateral displacements, thereby raising the likelihood of structural overturning. Field observations also revealed examples of vertical earthquake effects causing localized damage or progressive collapse. Fig. 30c shows steel columns subjected to buckling under high compressive forces, illustrating such cases. Additionally, buildings that lacked rigid diaphragm behavior or sufficient ductility at the structural level were significantly affected by vertical earthquake accelerations. For example, in buildings prone to torsional behavior due to irregular placement of shear walls and columns, localized damage in vertical load-bearing elements often led to rapid collapse in a manner consistent with the building's torsional mode, lacking ductile behavior. In Fig. 30d, the middle column of the rear facade in the +Y direction forms a plastic hinge, after which the building displaces in the -X and +Y directions, collapsing in a manner consistent with its torsional mode.

Additionally, evaluations were conducted in light of seismic fragility functions derived from previous research and the post-earthquake shakemap. Fragility functions, also referred to as vulnerability functions, estimate the probability of structural damage at a given level of seismic intensity. Exposure data, on the other hand, include information such as the building stock, population density, and economic values in the region. In this context, studies have been conducted to include the building stock in Türkiye, and vulnerability functions have been derived to obtain fragility curves. Following the 1999 Kocaeli earthquake, a risk assessment study was conducted, and fragility curves were developed for reinforced concrete frame structures in Türkiye with varying characteristics such as age and number of stories [80]. A similar study was carried out by Kircil and Polat [81], who examined the effect of the number of stories on the seismic fragility of reinforced concrete buildings constructed before the 2007 Turkish Earthquake Code [82]. Bilgin [83] further detailed the dataset and conducted fragility analyses, deriving different curves for reinforced concrete buildings. Usta and Bozdağ [84] focused on the seismic fragility of historical structures in Türkiye and developed fragility curves. More recently, the Federal Emergency Management Agency (FEMA) [85] has provided highly detailed data and fragility curves in its reports. In FEMA's study, fragility curves were developed for various building types, including historical masonry structures, steel structures, and reinforced concrete buildings with frame or shear wall systems. Parameters such as the number of stories and building age were also considered, and fragility curves were derived for four damage states: slight, moderate, extensive, and complete. In the present study, the compiled damage states were analyzed using these curves, and the fragility functions for reinforced concrete

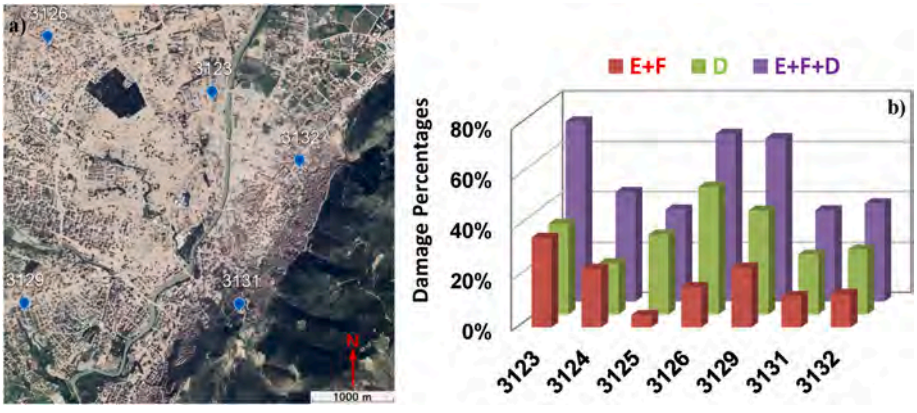

Fig. 29. a) Locations of Stations 3131–3132 [76], and b) building damage/destruction distributions.

Fig. 30. Views of damaged/collapsed buildings illustrating the vertical seismic effects [13].

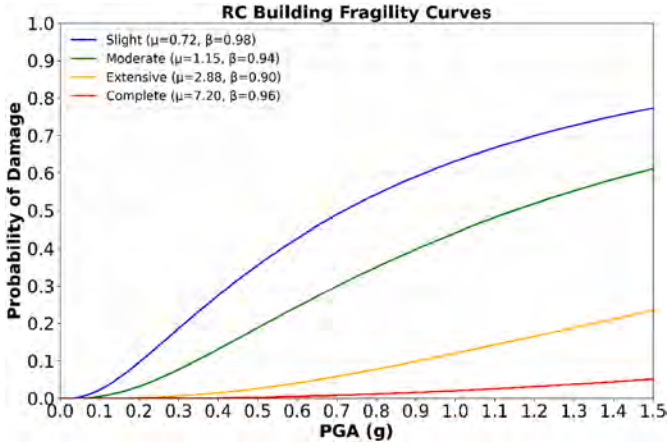

Fig. 31. Fragility curves provided by FEMA [85].

buildings were evaluated accordingly. Fig. 31 presents fragility curves for four different damage states: slight, moderate, extensive, and complete, as defined by FEMA. The lognormal distribution parameters for each damage state are shown in parentheses. The slight damage state represents very fine bending or shear cracks in some beams, columns, or joints. The complete damage state, on the other hand, is defined as brittle collapse or the loss of structural stability. The other damage states fall between these two extremes.

As shown in Table 3, the majority of buildings in the Antakya region are classified as aged (A) or moderately aged (M). This classification was considered when utilizing FEMA's fragility curves. For instance, the PGA value for Station 3123 is 0.668g, and even in the worst-case scenario fragility curves, the probabilities of extensive and complete damage for this PGA value did not exceed 10 %. However, it is evident that these probability estimates are underestimated when compared to the actual structural damage observed during the earthquake, indicating that these fragility curves are insufficient for accurately predicting the situation in Antakya. A similar observation applies to other recording stations (e.g., PGA: 1.234g for Station 3124; PGA: 1.379g for Station 3129, etc.). Besides, the shakemap, which illustrates the geographic distribution of ground shaking intensity following the earthquakes, further highlights the impact of the event in the region. Fig. 32 presents the ground shaking intensity map obtained after the February 6 earthquake, showing that the intensity and PGA values in the Antakya region were exceptionally high. This map also provides a clear understanding of the destruction and damage observed in the area.

6. Conclusions

This study focuses on the district of Antakya, one of the regions most affected by the February 6 Kahramanmaras earthquakes. Strong ground motion data from the Pazarcık earthquake, recorded at seismic stations located in Antakya, were analyzed. Potential supershear signatures, forward directivity, fling, basin effects, ground-motion amplification due to site-specific soil conditions, trampoline effects, and vertical ground accelerations were examined. Furthermore, the correlation between these phenomena and the observed damage in buildings near the station locations was investigated. The analysis yielded the following findings.

- The ground motions in the Antakya region carry the signatures of many intertwined phenomena due to the complex fault network, wave propagation, multi-segment rupture mechanisms, heterogeneous geological structure, geographical conditions, and topographic factors.
- In the analysis of ground motion data from the Antakya seismic stations, significant signs of a possible supershear effect were detected, particularly in the data from stations 3123, 3124, and 3129. Supershear signatures are faintly observed in the 3126 station records, but no strong traces are found in the 3125, 3131, and 3132 stations.
- When analyzing the velocity pulse characteristics in the ground motion records, it can be stated that effects such as forward directivity and fling coexist with supershear. The most important indicators leading to this conclusion are the correlations between the detected velocity pulse orientations and the seismic energy characteristics at different angles of the ground accelerations. By interpreting these connections through a combined supershear-directivity approach and assessing them through acceleration spectra, the possible supershear behavior along the fault-parallel direction can

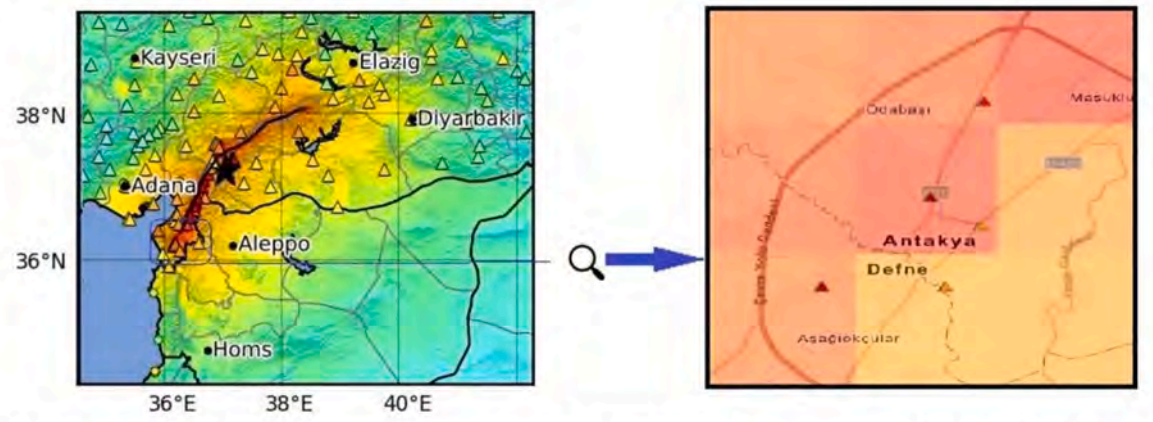

SHAKING	Not felt	Weak	Light	Moderate	Strong	Very strong	Severe	Violent	Extreme
DAMAGE	None	None	None	Very light	Light	Moderate	Moderate/heavy	Heavy	Very heavy
PGA(%g)	<0.0464	0.297	2.76	6.2	11.5	21.5	40.1	74.7	>139
PGV(cm/s)	<0.0215	0.135	1.41	4.65	9.64	20	41.4	85.8	>178
INTENSITY	I	II-III	IV	V	VI	VII	VIII	IX	X+

Fig. 32. Shakemap after Mw 7.8 Pazarcık event [86].

provide important insights. After the initial shock caused by the supershear effect, fault-normal pulse effects may emerge and, combined with directivity, create complex wave propagation patterns that generate different forms of ground motion. This phenomenon can explain the instabilities and orientation trends in the velocity pulse detections, the fault-parallel wave propagations that yield maximum CAV values, and the growth in spectral accelerations.

- As seen from the recorded acceleration values and response spectra at the stations, the role of the basin effect is significant in the high ground accelerations. The valley structure of the region and the alluvial sediments around the Asi River have created a suitable environment for the basin effect. As a result, the basin effects are quite evident, particularly around stations 3123, 3124, and 3129. Additionally, the north-south oriented mountain structure extending to the east and west of Antakya has led to a transition from soft to hard soil, resulting in seismic wave reflection phenomena.
- In regions that do not exhibit characteristics suitable for the basin effect, such as stations 3125, 3131, and 3132, the ground accelerations have not reached as high levels as at other stations. The beneficial contribution of the soil behavior, which does not amplify ground accelerations, is clearly visible in the 3131 and 3132 areas with hard soil conditions.
- The response spectra of the ground accelerations recorded at the Antakya station have often exceeded the DD1 design spectra proposed by TBDY-2018. This indicates the importance of the described phenomena in the observed ground accelerations. In future seismic hazard mapping studies within TBDY-2018, it would be appropriate to incorporate these effects into the probabilistic procedure to obtain more realistic elastic design spectra. In locations where near-fault effects are present, it is essential to deepen such studies and consider them in earthquake regulations.
- Similarly, vertical ground accelerations have reached very high values at almost all stations, surpassing the DD1 vertical design accelerations. The analyses indicate the presence of the trampoline effect in the region, which can be considered a contributing factor to the elevated vertical accelerations. Considering phenomena such as basin and trampoline effects, where the soil structure and behavior play a leading role, the approach of soil classification based on $V_{s,30}$ values used in structural design may be open to questioning. In cases involving complex effects, the realism of local soil coefficients, based on soil class in the prediction of design acceleration spectra, may deviate from reality. Therefore, it is clear that more detailed research on the soil is necessary to predict the role of the soil more accurately during the design phase.
- When the destruction and damage in the Antakya region after the Pazarcik earthquake are examined, the enhancing effects of parameters such as supershear, directivity, and basin effects on the damage can be observed. In the station areas that carry more combined traces of these effects, the destruction and damages have increased. Through visual inspections, considering the building stock's age, number of floors, and soil characteristics, the negative role of near-fault and soil effects has been numerically demonstrated through the percentages of damage and destruction.
- More detailed studies can be conducted by narrowing down the evaluation and conclusions in this study to the scale of a case study, and the results obtained can be revisited in future detailed analyses. It is clear that further investigation into the perspectives presented in this study through detailed modeling and analysis is necessary.
- In future studies, ground motion records can be analyzed in detail to parametrize the role of pulse-like effects and site behavior on the ground accelerations. The amplification mechanisms of these phenomena on seismic motions can be numerically defined, either as singular or coupled effects. Through this approach, different regional or multi-parameter site classifications could be developed, along with new procedures to incorporate these effects into design spectra. According to studies conducted using existing fragility functions, the damage level predictions for the Hatay region do not adequately reflect the actual conditions. Therefore, further research is needed to develop fragility analyses that can produce more realistic results. Additionally, the evaluations and conclusions presented in this study could be further deepened by refining the scope to specific case studies, and the findings could be reassessed through more advanced analyses in the future. It is clear that such detailed modeling and analysis are essential to thoroughly examine and validate the perspectives introduced in this study.

CRediT authorship contribution statement

Emre Gani: Writing – review & editing, Writing – original draft, Visualization, Resources, Project administration, Methodology, Investigation, Formal analysis, Data curation, Conceptualization. **Sezer Öztürk:** Writing – review & editing, Writing – original draft,

Methodology, Investigation, Data curation, Conceptualization. **Ali Sarı:** Validation, Supervision, Resources, Project administration, Methodology, Investigation, Data curation, Conceptualization.

Declaration of competing interest

The authors declare that they have no known competing financial interests or personal relationships that could have appeared to influence the work reported in this paper.

Data availability

Data will be made available on request.

References

[1] Baltzopoulos G, Baraschino R, Chioccarelli E, Cito P, Vitale A, Iervolino I. Near-source ground motion in the M7.8 Gaziantep (Turkey) earthquake. Earthq Eng Struct Dynam 2023;52(12):3903–12. https://doi.org/10.1002/eqe.3939.

[2] Duan Y, Bo J, Peng D, Li Q, Wan W, Qi W. Analysis of peak ground acceleration and seismogenic fault characteristics of the Mw7.8 earthquake in Turkey. Appl Sci 2023;13(19):10896. https://doi.org/10.3390/app131910896.

[3] Görüm T, Tanyas H, Karabacak F, Yılmaz A, Girgin S, Allstadt KE, et al. Preliminary documentation of coseismic ground failure triggered by the February 6, 2023 Türkiye earthquake sequence. Eng Geol 2023;327. https://doi.org/10.1016/j.enggeo.2023.107315.

[4] Istanbul Technical University. Final report, 6 Şubat 2023 04.17 Mw 7,8 kahramanmaraş (Pazarcık, Türkoglu), Hatay (Kırıkhan) ve 13.24 Mw 7,7 Kahramanmaraş (Elbistan/Nurhak-Çardak) Depremleri. https://haberler.itu.edu.tr/docs/default-source/default-document-library/2023_itu_deprem_on_raporu.pdf; 2023. 249. [accessed March 2023].

[5] Yetkin M, Dedeoğlu İÖ, Tunç G. Kahramanmaraş twin earthquakes: evaluation of ground motions and seismic performance of buildings for Elazığ, southeast of Türkiye. Soil Dynam Earthq Eng February 6, 2023;181. https://doi.org/10.1016/j.soildyn.2024.108678. 2024.

[6] Ivanov ML, Chow WK. Structural damage observed in reinforced concrete buildings in Adiyaman during the 2023 Turkiye Kahramanmaras Earthquakes. Structures 2023;58. https://doi.org/10.1016/j.istruc.2023.105578.

[7] Ince O. Structural damage assessment of reinforced concrete buildings in Adıyaman after Kahramanmaraş (Türkiye) Earthquakes on 6 February 2023. Eng Fail Anal 2024;156:107799. https://doi.org/10.1016/j.engfailanal.2023.107799.

[8] Kazaz İ, Avşar Ö, Dilsiz A. Importance of building inspection on the seismic response of a severely damaged RC structure during the February 6, 2023 Kahramanmaraş earthquake sequence. Eng Fail Anal 2024;162. https://doi.org/10.1016/j.engfailanal.2024.108410.

[9] Sezgin SK, Sakcalı GB, Özen S, Yıldırım E, Avcı E, Bayhan B, et al. Reconnaissance report on damage caused by the February 6, 2023, Kahramanmaraş Earthquakes in reinforced-concrete structures. J Build Eng 2024;89. https://doi.org/10.1016/j.jobe.2024.109200.

[10] Ozturk M, Arslan MH, Dogan G, Ecemis AS, Arslan HD. School buildings performance in 7.7 Mw and 7.6 Mw catastrophic earthquakes in southeast of Turkey. J Build Eng 2023;79. https://doi.org/10.1016/j.jobe.2023.107810.

[11] Ozkula G, Dowell RK, Baser T, Lin JL, Numanoglu OA, Ilhan O, et al. Field reconnaissance and observations from the February 6, 2023, Turkey earthquake sequence. Nat Hazards 2023;119(1):663–700. https://doi.org/10.1007/s11069-023-06143-2.

[12] Sagbas G, Sheikhi Garjan R, Sarikaya K, Deniz D. Field reconnaissance on seismic performance and functionality of Turkish industrial facilities affected by the 2023 Kahramanmaras earthquake sequence. Bull Earthq Eng 2023. https://doi.org/10.1007/s10518-023-01741-8.

[13] Altunsu E, Güneş O, Öztürk S, Sorosh S, Sarı A, Beeson ST. Investigating the structural damage in Hatay province after Kahramanmaraş-Türkiye earthquake sequences. Eng Fail Anal 2024;157. https://doi.org/10.1016/j.engfailanal.2023.107857.

[14] Arslan MH, Dere Y, Ecemiş AS, Doğan G, Öztürk M, Korkmaz SZ. Code-based damage assessment of existing precast industrial buildings following the February 6th, 2023 Kahramanmaraş earthquakes (Pazarcık Mw 7.7 and Elbistan Mw7.6). J Build Eng 2024;86. https://doi.org/10.1016/j.jobe.2024.108811.

[15] Kocaman İ, Mercimek Ö, Gürbüz M, Erbaş Y, Anıl Ö. The effect of Kahramanmaraş earthquakes on historical Malatya Yeni Mosque. Eng Fail Anal 2024;161. https://doi.org/10.1016/j.engfailanal.2024.108310.

[16] Nasery MM, Çelik M, Şadoğlu E. Damage assessment of Siverek Castle during the Kahramanmaraş earthquakes (Mw 7.7 and Mw 7.6) on 06 February 2023: remediation and strengthening proposals. Eng Geol 2024;334. https://doi.org/10.1016/j.enggeo.2024.107511.

[17] Öztürk S, Altunsu E, Güneş O, Sarı A. Investigation of industrial structure performances in the Hatay and Gaziantep provinces during the Türkiye earthquakes on February 6, 2023. Soil Dynam Earthq Eng 2024;179. https://doi.org/10.1016/j.soildyn.2024.108569.

[18] Chen G. Report on pulse-like ground motions in the Feb 2023 Turkey earthquakes. Hannover: Institute for Risk and Reliability Leibniz University; February 9, 2023. https://doi.org/10.13140/RG.2.2.31375.25767.

[19] Chang Z, Wu H, Li W, Yan Z, Peng L, Zhu G. Analysis of Near-Fault ground motions in the February 2023 kahramanmaras, Türkiye, earthquake sequence. Bull Earthq Eng 2025;23:1349–69. https://doi.org/10.1007/s10518-025-02101-4.

[20] Wu F, Xie J, An Z, Lyu C, Taymaz T, Irmak TS, et al. Pulse-like ground motion observed during the 6 February 2023 MW7.8 Pazarcık earthquake (Kahramanmaraş, SE Türkiye). Earthq Sci 2023;36(4):328–39. https://doi.org/10.1016/j.eqs.2023.05.005.

[21] Ertuncay D, Costa G. Analysis of impulsive ground motions from February 2023 Kahramanmaraş earthquake sequence. Bull Earthq Eng 2025;23:965–99. https://doi.org/10.1007/s10518-024-01897-x.

[22] Hu J, Liu M, Taymaz T, Ding L, Irmak TS. Characteristics of strong ground motion from the 2023 Mw 7.8 and Mw 7.6 Kahramanmaraş earthquake sequence. Bull Earthq Eng 2025;23:1225–54. https://doi.org/10.1007/s10518-023-01844-2.

[23] Melgar D, Taymaz T, Ganas A, Crowell B, Öcalan T, Kahraman M, et al. Sub- and super-shear ruptures during the 2023 Mw 7.8 and Mw 7.6 earthquake doublet in SE Türkiye. Seismica 2023;2(3). https://doi.org/10.26443/seismica.v2i3.387.

[24] Abdelmeguid M, Zhao C, Yalcinkaya E, Gazetas G, Elbanna A, Rosakis A. Dynamics of episodic supershear in the 2023 M7.8 Kahramanmaraş/Pazarcik earthquake, revealed by near-field records and computational modeling. Commun Earth Environ 2023;4(1). https://doi.org/10.1038/s43247-023-01131-7.

[25] Rosakis AJ, Abdelmeguid M, Elbanna A. Evidence of early supershear transition in the Mw 7.8 Kahramanmaraş earthquake from near-field records. Preprint, https://doi.org/10.31223/X5W95G; 2023.

[26] Okuwaki R, Yagi Y, Taymaz T, Hicks SP. Multi-scale rupture growth with alternating directions in a complex fault network during the 2023 south-eastern Türkiye and Syria earthquake doublet. Geophys Res Lett 2023;50(12). https://doi.org/10.1029/2023GL103480.

[27] Karray M, Karakan E, Kincal C, Chiaradonna A, Gül TO, Lanzo G, et al. Türkiye Mw 7.7 Pazarcık and Mw 7.6 Elbistan earthquakes of February 6th, 2023: contribution of valley effects on damage pattern. Soil Dynam Earthq Eng 2024;181. https://doi.org/10.1016/j.soildyn.2024.108634.

[28] Işık NS. Basin and Near-Fault effects on earthquake ground motions: an evaluation of the Antakya records of the Kahramanmaraş Pazarcık earthquake. J Geol Eng 2023;47:67–86. https://doi.org/10.24232/jmd.1299027.

[29] Ilhan O, Indır O, Muratoğlu G, İçen A, Albayrak K, Sandıkkaya MA, et al. Local site effects at the selected stations affected by the February 6 2023 Türkiye Earthquake Sequences. Soil Dynam Earthq Eng 2024;178. https://doi.org/10.1016/j.soildyn.2024.108454.

[30] Aoi S, Kunugi T, Fujiwara H. Trampoline effect in extreme ground motion. Science 2008;322(5902):727–30. https://doi.org/10.1126/science.1163113.

[31] Türkiye Building Earthquake Code (TBEC-2018). Republic of Türkiye ministry of interior disaster and emergency management authority. 2018. Ankara.

[32] Yaghmaei-Sabegh S, Neekmanesh S, Ruiz-García J. Evaluation of vertical-to-horizontal spectral acceleration ratio for the 2023 Turkey-Syria seismic sequences. Soil Dynam Earthq Eng 2024;182. https://doi.org/10.1016/j.soildyn.2024.108747.

[33] Iervolino I, Baltzopoulos G, Chioccarelli E, Suzuki A. Seismic actions on structures in the near-source region of the 2016 central Italy sequence. Bull Earthq Eng 2019;17:5429–47. https://doi.org/10.1007/s10518-017-0295-3.

[34] Iervolino I, Giorgio M, Cito P. Which earthquakes are expected to exceed the design spectra? Earthq Spectra 2019;35(3):1465–83. https://doi.org/10.1193/032318EQS066O.

[35] Wikipedia. Hatay'ın ilçeleri. https://tr.wikipedia.org/wiki/Hatay%27%C4%B1n_il%C3%A7eleri/. [Accessed 15 January 2025].

[36] Ministry of Environment. Urbanization and climate change of the republic of Türkiye. Damage Assess Inq 2024. 2024. Available at: https://hasartespit.csb.gov.tr/. January 2024.

[37] Somerville PG. "Engineering characterization of near fault ground motions". Wellington, New Zealand: New Zealand Society for Earthquake Engineering, NZSEE Conference. 11 March 2005, https://db.nzsee.org.nz/2005/Paper01.pdf; 2005.

[38] Baker JW. Quantitative classification of near-fault ground motions using wavelet analysis. Bull Seismol Soc Am 2007;97(5):1486–501. https://doi.org/10.1785/0120060255.

[39] Shahi SK, Baker JW. An efficient algorithm to identify strong-velocity pulses in multicomponent ground motions. Bull Seismol Soc Am 2014;104(5):2456–66. https://doi.org/10.1785/0120130191.

[40] Chang Z, Wu H, Goda K. Automated parameterization of velocity pulses in near-fault ground motions. Earthq Eng Struct Dynam 2024;53(3):1006–27. https://doi.org/10.1002/eqe.4053.

[41] Gabor D. Theory of communication. Part 1: the analysis of information. J Inst Electr Eng Part III Radio Commun Eng 1946;93(26):429–41. https://doi.org/10.1049/ji-3-2.1946.0074.

[42] Levy D. A century after the 1906 earthquake, geophysicists revisit "The Big One" and come up with a new model. Stanford University; 2 December, 2005. https://web.archive.org/web/20080129092039/http://news-service.stanford.edu/pr/2005/pr-agu_beroza-120705.html/. January 2025.

[43] Ren C, Wang Z, Taymaz T, Hu N, Luo H, Zhao Z, et al. Supershear triggering and cascading fault ruptures of the 2023 Kahramanmaraş, Türkiye, earthquake doublet. Science 2024;383(6680):305–11. https://doi.org/10.1126/science.adi1519.

[44] Towhata I, Çağlayan PÖ, Tönük G, Erginağ UC, Torisu SS. Reconnaissance and discussion on ground motion induced by the 2023 Türkiye-Syria earthquake.

J Earthq Eng 2025;29(5):981–1022. https://doi.org/10.1080/13632469.2025.2458600.
[45] Andrews DJ. Rupture velocity of plane strain shear cracks. J Geophys Res 1976;81(32):5679–87. https://doi.org/10.1029/JB081i032p05679.
[46] Burridge R, Conn G, Freund LB. The stability of a rapid mode II shear crack with finite cohesive traction. J Geophys Res 1979;84(B5):2210–22. https://doi.org/10.1029/JB084iB05p02210.
[47] Honda H. On the initial motion and the types of the seismograms of the north Idu and the Itô earthquakes. Geophys Magazine Central Meteorol Observ Jpn 1931;4(3):185–213.
[48] Honda H. On the initial motion and the types of the seismograms of the north Idu and Ito earthquakes. J Meteorol Soc Jpn 1932;9(7):293–314 (in Japanese).
[49] Maruyama T. On the force equivalents of dynamic elastic dislocations with reference to the earthquake mechanisms. Bull Earthq Res Inst 1963;41(3):467–86.
[50] Mello M, Bhat HS, Rosakis AJ. Spatiotemporal properties of Sub-Rayleigh and supershear rupture velocity fields: theory and experiments. J Mech Phys Solid 2016;93:153–81. https://doi.org/10.1016/j.jmps.2016.02.031.
[51] Delouis B, Ende M, Ampuero JP. Kinematic rupture model of the February 6th, 2023, Mw7.8 Turkey earthquake from a large set of near-source strong motion records combined by GNSS offsets reveals intermittent supershear rupture. Bull Seismol Soc Am 2024;114(2):726–40. https://doi.org/10.1785/0120230077.
[52] Lee SJ, Liu TY, Lin TC. Abnormal apparent supershear rupture with discontinuous jumping propagation during the 2023 Türkiye M7.8 earthquake. Commun Earth Environ 2024;5(1). https://doi.org/10.1038/s43247-024-01481-w.
[53] Xu L, Mohanna S, Meng L, Ji C, Ampuero JP, Yunjun Z, et al. The overall-subshear and multi-segment rupture of the 2023 Mw7.8 Kahramanmaraş, Turkey earthquake in millennia supercycle. Commun Earth Environ 2023;4:379. https://doi.org/10.1038/s43247-023-01030-x.
[54] Över S, Büyüksaraç A, Bekta Ö, Filazi A. Assessment of potential seismic hazard and site effect in Antakya (Hatay Province), SE Turkey. Environ Earth Sci 2011;62(2):313–26. https://doi.org/10.1007/s12665-010-0525-3.
[55] Cakti E, Bikce M, Ozel O, Genes C, Kacin S, Kaya Y. Antakya basin strong ground motion network. Geophys Res Abstr 2011;13.
[56] Topographic map of Hatay. Topographic map. Available at: https://en-gb.topographic-map.com/; 2025. April 2025.
[57] Kale Ö, Akkar S, Ansari A, Hamzehloo H. A ground-motion predictive model for Iran and Turkey for horizontal PGA, PGV, and 5% damped response spectrum: investigation of possible regional effects. Bull Seismol Soc Am 2015;105(2A):963–80. https://doi.org/10.1785/0120140134.
[58] Akkar S, Sandıkkaya MA, Şenyurt M, Azari Sisi A, Ay BÖ, Treversa P, et al. Reference database for seismic ground motion in Europe (RESORCE). Bull Earthq Eng 2014;12:311–39. https://doi.org/10.1007/s10518-013-9506-8.
[59] Boore DM, Stewart JP, Seyhan E, Atkinson GM. NGA-West 2 equations for predicting PGA, PGV, and 5%-damped PSA for shallow crustal earthquakes. Earthq Spectra 2014;30:1057–85. https://doi.org/10.1193/070113EQS184M.
[60] Disaster and Emergency Management Authority (AFAD). Turkish accelerometric database and analysis system (TADAS). Available at: https://tadas.afad.gov.tr/login/; 2025. January 2025.
[61] General directorate of mineral research and exploration (MTA), Amanos fault segment. Available at: https://www.mta.gov.tr/; 2024. December 2024.
[62] Bouchon M, Bouin MP, Karabulut H, Toksöz MN, Dietrich M, Rosakis AJ. How fast is rupture during an earthquake? New insights from the 1999 Turkey earthquakes. Geophys Res Lett 2001;28(14):2723–6. https://doi.org/10.1029/2001GL013112.
[63] Nemutlu ÖF, Sarı A, Balun B. Estimation of seismic effective energy based parameter. Struct Eng Mech 2022;82(6):785–99. https://doi.org/10.12989/sem.2022.82.6.785.
[64] Howard JK, Tracy CA, Burns RG. Comparing observed and predicted directivity in near-source ground motion. Earthq Spectra 2005;21(4):1063–92. https://doi.org/10.1193/1.2044827.
[65] Yang D, Zhou J. A stochastic model and synthesis for near-fault impulsive ground motions. Earthq Eng Struct Dynam 2015;44(2):243–64. https://doi.org/10.1002/eqe.2468.
[66] Wu G, Zhai C, Li S, Xie L. Effects of near-fault ground motions and equivalent pulses on large crossing transmission tower-line system. Eng Struct 2014;77:161–9. https://doi.org/10.1016/j.engstruct.2014.08.013.
[67] Li C, Zuo Z, Kunnath S, Chen L. Orientation of the strongest velocity pulses and the maximum structural response to pulse-like ground motions. Soil Dynam Earthq Eng 2020;136. https://doi.org/10.1016/j.soildyn.2020.106240.
[68] Mello M, Bhat HS, Rosakis AJ, Kanamori H. Reproducing the supershear portion of the 2002 Denali earthquake rupture in laboratory. Earth Planet Sci Lett 2014;387:89–96. https://doi.org/10.1016/j.epsl.2013.11.030.
[69] Dunham EM, Bhat HS. Attenuation of radiated ground motion and stresses from three-dimensional supershear ruptures. J Geophys Res Solid Earth 2008;113(8). https://doi.org/10.1029/2007JB005182.
[70] Papazafeiropoulos G, Plevris V. Kahramanmaraş—Gaziantep, Türkiye Mw 7.8 earthquake on 6 February 2023: strong ground motion and building response estimations. Buildings 2023;13(5). https://doi.org/10.3390/buildings13051194.
[71] Newmark NM, Blume JA, Kapur KK. Seismic design spectra for nuclear power plants. J Power Div 1973;99(2):287–303.
[72] Papazoglou AJ, Elnashai AS. Analytical and field evidence of the damaging effect of vertical earthquake ground motion. Earthq Eng Struct Dynam 1996;25(10):1109–37. https://doi.org/10.1002/(SICI)1096-9845(199610)25:10<1109::AID-EQE604>3.0.CO;2-0.
[73] International Building Code (IBC). As mandated and incorporated by the states and municipalities and by the code of federal regulations at 36 CFR 1191. 2000.
[74] American Society of Civil Engineers (ASCE). Minimum design loads and associated criteria for buildings and other structures, ASCE/SEI 7-16. Am Soc Civ Eng 2017. Reston, VA.
[75] Tobita T, Iai S, Iwata T. Numerical analysis of trampoline effect in extreme ground motion. San diego, California: fifth international conference on recent advances in geotechnical earthquake engineering and soil dynamics and symposium in honor of Prof. I. M. Idriss; 2010. May 2010. p. 24–9.
[76] Google. Google Earth. Available at: https://earth.google.com/web/; 2025. January 2025.
[77] General Directorate of Land Registry and Cadastre. Parcel query application. Available at: https://parselsorgu.tkgm.gov.tr/; 2024. November 2024.
[78] Google. Google maps. Available at: https://www.google.com/maps/; 2024. November 2024.
[79] Global Vs30 Mosaic. Türkiye major fault lines map. Available at: https://mapelse.github.io/global_vs30/; 2024. November 2024.
[80] Erdik M, Aydinoglu N, Fahjan Y, Sesetyan K, Demircioglu M, Siyahi B, et al. Earthquake risk assessment for Istanbul metropolitan area. Earthq Eng Eng Vib 2003;2(1):1–23. https://doi.org/10.1007/BF02857534.
[81] Kirçil MS, Polat Z. Fragility analysis of mid-rise R/C frame buildings. Eng Struct 2006;28:1335–45. https://doi.org/10.1016/j.engstruct.2006.01.004.
[82] TEC-2007. Turkish earthquake code: specification for structures to be built in disaster areas. Turkish Ministry of Environment and Urban Planning; 2007. Ankara, Türkiye (, in Turkish).
[83] Bilgin H. Fragility-based assessment of public buildings in Turkey. Eng Struct 2013;56:1283–94. https://doi.org/10.1016/j.engstruct.2013.07.002.
[84] Usta P, Bozdağ Ö. Seismic fragility analysis of traditional himis structures in Turkey. Structures 2022;43:28–39. https://doi.org/10.1016/j.istruc.2022.06.028.
[85] FEMA. Hazus earthquake model technical manual, Hazus 6.1. Federal Emergency Management Agency; July 2024.
[86] USGS. Macroseismic intensity map. Feb 06 2023 01:17:34. United States Geological Survey; 2023. https://earthquake.usgs.gov/earthquakes/eventpage/us6000jllz/shakemap/intensity/. April 2025.